

Inclusive scattering data on light nuclei as a tool for the extraction of G_M^n

A.S. Rinat and M.F. Taragin

Weizmann Institute of Science, Department of Particle Physics, Rehovot 76100, Israel

M. Viviani

INFN, Sezione Pisa and Phys. Dept., University of Pisa, I-56100, Italy

(Dated: August 10, 2018)

We demonstrate that refinements in the analysis of inclusive scattering data on light nuclei enable the extraction of, generally accurate, values of the neutron magnetic form factor $G_M^n(Q^2)$. In particular, a recent parametrization of ep inclusive resonance excitation enables a reliable calculation of the inelastic background, and as a consequence a separation of quasi-elastic and inelastic contributions. A far larger number of data points than previously considered is now available for analysis and enables a more reliable extraction of G_M^n from cross section and R_T data on D and He. The achieved accuracy appears mainly limited by the present uncertainties in the knowledge of proton form factors and by the accuracy of the data.

I. INTRODUCTION.

In a previous report we discussed the feasibility to extract the neutron magnetic form factor (FF) $G_M^n(Q^2)$ from inclusive electron scattering data on D and ^4He [1] at small and moderate Q^2 . Using a simple model for inclusive resonance excitation, we established, that in the immediate vicinity of the quasi-elastic peak (QEP), the QE components dominate the inelastic background, which was subsequently neglected. That procedure severely restricts the number of data points around the QEP available for the extraction of $\alpha_n = G_M^n/\mu_n G_d$ (μ_n and $G_d(Q^2) = [1 + Q^2/0.71]^{-2}$ are the static magnetic moment of the neutron, and the standard dipole form factor).

For several reasons we propose to extend the above analysis:

1) Availability of an unpublished set of low- Q^2 quasi-elastic (QE) data on ^4He , [2], which are contained in a PhD Thesis of J-P. Chen [3] and which cover a nearly continuous range in Q^2 . Moreover, contrary to the older NE3 data [4], most of the NE9 data sets reach, or extend into the resonance region.

2) After completion of Ref. 1 we have been informed of recent high-quality inclusive resonance excitation data on a proton, which supersede parameterizations of older SLAC [5] and of more recent JLab data [6] (see also Ref. [7]). In addition a model has to be devised in order to obtain the required neutron structure functions (SF) F_k^n ($k = 1, 2$) [8], which appears in the desired F_k^N , the averaged p, n SF. The latter is related to the nuclear SF F_k^A by means of $f^{PN,A}$, the SF of a fictitious nucleus composed of point-nucleons, which has to be computed.

The above F_k^N may be separated into nucleon-elastic (NE) and nucleon-inelastic (NI) components $F_k^{N,NE}, F_k^{N,NI}$, which correspond to processes where, after absorption of a virtual photon, the nucleon is not, or gets excited. The above mentioned relation generates a similar division of the nuclear SF $F_k^A = F_k^{A,NI} + F_k^{A,NE}$.

In each data set we consider two regions:

A) The high energy-loss region far from the QEP, which is dominated by the nuclear NI background: Tails of QE contributions barely depend on the precise value of G_M^n and, the overwhelmingly inelastic computed cross sections can thus be compared against data.

B) With decreasing energy loss one reaches the inelastic and elastic sides of the QEP. There we focus on the difference between data and the NI components. To those we apply a criterion which, when fulfilled, identifies the above differences as $F_k^{A,NE}$, which is related to the nucleon FFs. The QE region will be shown to be the most sensitive one for variations in α_n , and is hence the area of prime interest.

The above program is hampered by complicating circumstances. Foremost is the discrepancy [9, 10] between the G_E^p/G_M^p ratio, extracted from Rosenbluth-separated elastic ep cross sections and from $\vec{e}(p, \vec{p})e$ polarization transfer data [11, 12]. At this time it is not obvious which p FFs should be used. It seems that two-photon exchange contributions [13, 14] confirm the E/M ratio for the proton, provided by the polarization transfer data. Unfortunately this does not directly reflect on the FFs themselves, because the ep data have as yet not been corrected for those contributions, prior to an extraction. Before resolution of the above issue, a choice for the required input will have to be made. Arrington recommends the use of the experimentally simplest, non-separated ep cross section data.

The present note is organized as follows. We start with total inclusive cross sections, but shall also re-analyze the components for the absorption of virtual transverse photons $\propto R_T$. After discussing the required input, we analyze all good-quality data on D, ^4He .

We first concentrate on the region below and around the QEP, where NE components generally dominate. This enables one to reliably extract α_n from any given data set. We no more neglect NI, as had previously been done [1],

and instead subtract those from the data in order to isolate the NE components. We also show that the computed cross sections agree very well with the data in and beyond the resonance region, which are completely dominated by NI components. Between the inelastic slope of the QE region and the elastic wing of the resonance region, the NI components falls short of their predictions and we discuss a possible origin.

In the discussion we set limits to the accuracy of the results, caused by occasionally data of insufficient quality, the ambiguity of the proton FFs, and uncertainty in the NI components. Without substantial improvements in each of the above items, we do not envisage the possibility to substantially improve the results of the model.

II. QUASI-ELASTIC INCLUSIVE SCATTERING.

Consider the cross section per nucleon for inclusive scattering over an angle θ of unpolarized electrons with energy E

$$\frac{d^2\sigma^A(E; \theta, \nu)}{d\Omega d\nu} = \sigma_M(E; \theta, \nu) \left[\frac{2xM}{Q^2} F_2^A(x, Q^2) + \frac{2}{M} F_1^A(x, Q^2) \tan^2(\theta/2) \right], \quad (2.1)$$

with σ_M , the Mott cross section. Above, $F_{1,2}^A(x, Q^2)$ are the nuclear SF, depending on the squared 4-momentum transfer $q^2 = -Q^2 = -(|\mathbf{q}|^2 - \nu^2)$ and the Bjorken variable $x = Q^2/2M\nu$, with M the nucleon mass. Its range is $0 \leq x \leq A$.

In an alternative representation

$$\frac{d^2\sigma^A}{d\Omega d\nu} = \sigma_M [W_2^A + 2W_1^A \tan^2(\theta/2)] \quad (2.2)$$

$$= \sigma_M \frac{Q^2}{|\mathbf{q}|^2} [W_L^A + \epsilon^{-1} W_T^A] \equiv \sigma_M \frac{Q^2}{|\mathbf{q}|^2} \left[\frac{Q^2}{|\mathbf{q}|^2} R_L^A + \frac{1}{2} \epsilon^{-1} R_T^A \right], \quad (2.3)$$

where $\epsilon^{-1} = 1 + 2(|\mathbf{q}|^2/Q^2) \tan^2(\theta/2)$. The SF W_L^A, W_T^A (2.3) relate to the absorption of longitudinal and transverse photons.

In the sequel we shall use a relation between SF $F_k^{N,A}$ for nucleons ($N = p, n$) and a nucleus which, for isospin $I = 0$ targets of our interest, reads [15]

$$F_k^A(x, Q^2) = \int_x^A \frac{dz}{z^{2-k}} f^{PN,A}(z, Q^2) \sum_l C_{kl}(z, Q^2) \left[F_l^p\left(\frac{x}{z}, Q^2\right) + F_l^n\left(\frac{x}{z}, Q^2\right) \right] / 2 \quad (2.4)$$

The link between $F^N = (F^p + F^n)/2$ and F^A is provided by $f^{PN,A}$, the SF of a fictitious target A , which is composed of point-nucleons. Eq. (2.4) holds in the Bjorken limit $Q^2 \rightarrow \infty$, as well as in the Plane Wave Impulse Approximation (PWIA).

For quite some time we have considered Eq. (2.4) for finite Q^2 in an alternative, non-perturbative approach [15], based on a covariant generalization [16] of the non-relativistic theory of Gersch-Rodriguez-Smith (GRS) [17]. We considered the above as a conjecture, and its apparent validity for $Q^2 \gtrsim Q_0^2 \approx 2.5 \text{ GeV}^2$ as an empirical fact [18].

Only recently did we come across work by West and Jaffe who more than 20 years ago proved Eq. (2.4) in the PWIA, using either a parton model or pQCD [19, 20]. It is actually possible to generalize their proof by adding Final State Interactions (FSI) to the PWIA, reaching the Distorted Wave Impulse Approximation. The same holds for the inclusion of FSI in the GRS version [21] and the proof formally recovers Eq. (2.4). The intriguing difference lies in the interpretation: in the effective hadronic description one uses typical nuclear concepts, as are nuclear density matrices, effective NN scattering amplitudes, etc. Those are of course foreign concepts in QCD. Similar remarks hold for recently discussed effective nuclear parton distribution functions [22].

We return to Eq. (2.4), which includes the effect of mixing of the nucleon SF embodied in the coefficients C_{kl} [23, 24]. In both the PWIA and the GRS approach, $C_{11} = 1$, $C_{12} = 0$, while C_{21} is negligibly small. For a discussion of an approximate fashion to compute C_{22} in the GRS, we refer to Appendix A of Ref. 1. Since the approximately calculated deviation of C_{22} from 1 does not decrease fast enough with Q^2 , we use $C_{22}(Q^2) \rightarrow 1$ for $Q^2 \gtrsim 3.5 \text{ GeV}^2$.

Finally we remark that Eq. (2.4) relates to nucleons as the dominant source of partons. This is the case for $x \gtrsim 0.20$ [25] and thus certainly for the range on which we focus $0.4 \lesssim x \lesssim 1.2$, which comprises the QEP.

Next we recall the NE and NI parts $F_k^{N,NE}, F_k^{N,NI}$ of nucleon SF, which correspond to the elastic absorption of a virtual photon on a $N \gamma^* + N \rightarrow N$ and to inelastic absorption $\gamma^* + N \rightarrow (\text{hadrons, partons})$. Elastic components

for a nucleon vanish except for $x = 1$ and contain the standard combinations of the electro-magnetic FF $G_{E,M}^N(Q^2)$. Denoting the average of their squares by $[\tilde{G}^N]^2 = [(G^p)^2 + (G^n)^2]/2$, one has ($\eta = Q^2/(4M^2)$)

$$F_1^{N,NE}(x, Q^2) = \frac{1}{2}\delta(1-x)[\tilde{G}_M^N(Q^2)]^2 \quad (2.5)$$

$$F_2^{N,NE}(x, Q^2) = \delta(1-x) \frac{[\tilde{G}_E^N(Q^2)]^2 + \eta[\tilde{G}_M^N(Q^2)]^2}{1 + \eta} \quad (2.6)$$

It is a trivial matter to express the corresponding NE, NI parts of *nuclear* SF F_k^A , using the link (2.4) in its region of validity $x \gtrsim 0.2$. Thus for the nuclear NE (QE) parts

$$F_1^{A,NE}(x, Q^2) = \frac{f^{PN,A}(x, Q^2)}{2} [\tilde{G}_M^N(Q^2)]^2 \quad (2.7)$$

$$F_2^{A,NE}(x, Q^2) = x f^{PN,A}(x, Q^2) C_{22}^A(x, Q^2) \frac{[\tilde{G}_E^N(Q^2)]^2 + \eta[\tilde{G}_M^N(Q^2)]^2}{1 + \eta} \quad (2.8)$$

Since $f^{PN,A}$ for light nuclei is sharply peaked around $x \approx 1$, the same holds for $F_k^{A,NE}$. For the L, T components corresponding to Eqs. (2.5), (2.6) one has

$$R_T^{N,NE}(x, Q^2) = \delta(1-x) \frac{[\tilde{G}_M^N]^2}{M} \quad (2.9)$$

$$R_L^{N,NE}(x, Q^2) = \delta(1-x) \frac{(1 + \eta)[\tilde{G}_E^N]^2}{2M\eta} \quad (2.10)$$

Clearly the NE L, T components for the N separate magnetic and electric FF. However, the generalization of the above to composite targets depends on the model which relates NE parts of the nucleon and target SF. In the GRS approach one finds from Eqs. (2.4), (2.9) and (2.10)

$$R_T^{A,NE} = \frac{f^{PN,A}}{M} [\tilde{G}_M^N]^2 \quad (2.11)$$

$$R_L^{A,NE} = \left(1 + \frac{\eta}{x^2}\right) \frac{f^{PN,A}}{2M(1 + \eta)} \left[\left\{ C_{22} \left(\frac{x^2}{\eta} + 1 \right) \right\} [\tilde{G}_E^N]^2 + \left\{ (C_{22} - 1)(x^2 + \eta) + x^2 - 1 \right\} [\tilde{G}_M^N]^2 \right] \quad (2.12)$$

The NE part of the transverse nuclear SF still contains only magnetic FFs. However, for the model defined by Eq. (2.4) the longitudinal nuclear partner $R_L^{A,NE}$, Eq. (2.12) is generally a combination of E, M FFs, except at the position $x = 1$ of the unshifted QEP, and then only for unmixed F_k^A in Eq. (2.4), i.e. with $C_{22} = 1$. The above contrasts with the PWIA, where no such mixture occurs in $R_L^{A,NE}$. Only in a very limited number of inclusive scattering experiments have Rosenbluth L, T separations been performed. As a consequence most of our efforts are concentrated on the more involved total inclusive data.

When focusing on FFs, one has to isolate in the data the NE parts (2.7), (2.8), which contain those FFs. Such a procedure obviously requires accurate knowledge of the nuclear NI background in the QE region $x \approx 1$, and which on the adjacent inelastic side of the QEP $x \lesssim x_0(Q^2) \lesssim 1$, is dominated by inclusive resonance excitation.

Just as the NE components in $F_k^{N,NE}$ produce in nuclei the corresponding $F_k^{A,NE}$, which is centered around the QE peak, also N -resonances in $F_k^{N,NI}$ may be reflected in nuclei SF $F_k^{A,NI}$. In particular for $A \leq 4$, for which $f^{PN,A}$ is sharply peaked in x , both $F_k^{N,NI}$ and $F_k^{A,NI}$ have maxima at about the same x . We recall, that the observed structures in $F_k^{A,NI}$ for $Q^2 \leq 3 \text{ GeV}^2$ and $\nu > \nu_{\text{QEP}}$, are *not* genuine target resonances but nucleon resonances, modified by the nuclear medium [26]. We refer to those structures as 'pseudo-resonances' [27].

We conclude this section returning to the validity of Eq. (2.4). The simple forms (2.7) and (2.8) for the nuclear NE parts hold quite generally, even below the estimated $Q_0^2 \approx 2.5 \text{ GeV}^2$. The same may be assumed for the NI part, due to the inclusive excitation of very narrow resonances. With some hesitation we shall therefore make applications even for $Q^2 = 0.5 \div 1 \text{ GeV}^2$, but one should be prepared to encounter less good fits for those, than for larger Q^2 .

III. INPUT.

We review major theoretical input elements:

1) Density matrices for the target nuclei, diagonal in all coordinates except one. Those relate to ground state wave functions and have for the lightest nuclei been calculated with great precision [28, 29]. For heavier targets one has to invoke approximations, for instance by interpolation between diagonal density matrices and special limiting situations [17, 30]. Wishing to avoid theoretical uncertainties, we do not incorporate in our analysis data for targets with $A \geq 12$.

2) NN dynamics for Final State Interactions (FSI) [30], which enters the calculation of $f^{PN,A}$.

3) $F_k^{p;NI}$: We considered various representations for F_k^p , all having explicit resonance and background components, namely Stuart *et al* [5] and more recent ones 'christy1' and 'christy2' [6], based on Rosenbluth-separated cross sections (cf. also [7]). The second version is claimed to be of somewhat better quality. However, the argument x/z of the latter in Eq. (2.4) varies for fixed Q^2 and occasionally crosses stated regions of validity. The ensuing inconsistencies appear more severe for christy2 than for christy1 and we thus prefer the latter. Since the parameterizations are of relatively poorest quality for small Q^2 , one should expect correspondingly inferior results.

For large Q^2 one avoids uncertainties and even inconsistencies by choosing a fixed $Q^2 = 3.5 \text{ GeV}^2$, beyond which we switch to a parametrization of F_2^p , averaged over resonances [31]. For F_1^p at high Q^2 we employ those of Bodek-Ritchie [32]. The chosen procedure is in line with quark-hadron duality, which predicts similar outcome for F_k^N , both globally, when averaged over the entire resonance region [33], and locally for isolated resonances [34, 35].

4) $F_k^{n;NI}$: We use a procedure presented in Ref. 8, based on the ratio

$$\begin{aligned} \mathcal{C}(x, Q^2) &= F_2^n(x, Q^2)/F_2^p(x, Q^2) \\ &\equiv \sum_{k=0}^2 d_k(Q^2)(1-x)^k, \end{aligned} \quad (3.1)$$

with the coefficients $d_k(Q^2)$ to be determined by information on \mathcal{C} for 3 selected points:

- i) $\mathcal{C}(0, Q^2) = 1$, required to obtain a finite Gottfried sum [8].
- ii) Use of the primitive choice $F^n = 2F^D - F^p$, which is accurate for $x \leq 0.3$ and is exploited for the value $x = 0.2$.
- iii) Information from the elastic end-point $x = 1$, where \mathcal{C} is determined by static FF

$$\mathcal{C}(1, Q^2) = \frac{\left[G_E^n(Q^2) \right]^2 + \eta \left[G_M^n(Q^2) \right]^2}{\left[G_E^p(Q^2) \right]^2 + \eta \left[G_M^p(Q^2) \right]^2}. \quad (3.2)$$

We assume the same \mathcal{C} for an estimate of F_1^n from F_1^p : Eq. (3.1) then provides $F_{k=1,2}^N(x, Q^2)$. The latter and the computed $f^{PN,A}$ are from Eq. (2.4) seen to be input for the calculation of nuclear SF F_k^A .

Note that Eq. (3.2) for $\mathcal{C}(1, Q^2)$ requires also G_M^n , the very FFs we wish to extract. Fortunately, for not too large Q^2 the ratio in Eq. (3.2) depends only marginally on G_M^n . Solely in order to determine $\mathcal{C}(1, Q^2)$, we use in Eq. (3.2) the parametrization of G_M^n given in Ref. 36: we do not demand self-consistency.

5) Electromagnetic FFs: In Ref. 1 we had adopted the ratio

$$\begin{aligned} \gamma &= \frac{G_E^p}{(G_M^p \mu_p)} \\ &= 1 \quad \text{for } Q^2 \lesssim 0.3 \text{ GeV}^2, \quad \text{choice I,} \\ &\approx [1 - 0.14(Q^2 - 0.3)] \quad \text{for } 0.3 \lesssim Q^2 \lesssim 5.5 \text{ GeV}^2 \end{aligned} \quad (3.3)$$

from polarization transfer in $\vec{e}(p, \vec{p})e$ [11, 12], $\alpha_p = G_E^p/(\mu_p G_d)$.

For all but the smallest Q^2 , the above mentioned E/M ratio for the p FFs's disagrees substantially from results from Rosenbluth-separated elastic ep data [37, 38]. Two-photon exchange contributions have been computed [13], but those have as yet not been extracted from data in order to re-analyze the extraction of FFs.

It is therefore impossible at this moment to make an impartial choice for p FFs, and we shall report results for two sets of extracted α_n : 'I', based on the ratio (3.3) and 'II', using cross section data. We adopt the recommended parameterizations of $G_{E,M}^p$ [36]

$$G_{E,M}^p(Q^2) = G_{E,M}^p(0) \left/ \left[1 + \sum_{m=1} a_m^p(Q^2)^m \right] \right., \quad \text{choice II.} \quad (3.4)$$

A previously used parametrization for α_p [39] is close to one of the form (3.4) (see Table 2 in Ref. 36).

There is still lacking reliable data for G_E^n beyond relatively low Q^2 [40]. Analyses continue to prefer a Galster-like form

$$G_E^n(Q^2) = -\mu_n G_d(Q^2) \frac{A\eta}{1 + B\eta}, \quad (3.5)$$

with $A = 0.942, B = 4.61$ [41, 42, 43]. Two recent, more precise measurements yield $A = 0.888, B = 3.21$ [44]. Differences do no amount too much for the small measured Q^2 : for larger Q^2 , where G_E^n grows in relative importance, there is no way to prefer one particular assumed extrapolation.

IV. GENERAL OBSERVATIONS AND EXTRACTION PROCEDURE.

We start with the NE parts of inclusive cross sections and remark on two samples for quite different Q^2 , namely ${}^4\text{He}$ ($E = 3.6 \text{ GeV}, \theta = 15^\circ, Q^2 \approx 0.973 \text{ GeV}^2$) and D ($E = 4.045 \text{ GeV}, \theta = 30^\circ, Q^2 \approx 2.77 \text{ GeV}^2$). Figs. 1,2 show on a linear scale the cross section data (solid circles), the calculated NI background (dotted curves) and $\sigma^{A,NE}$ computed for some α_n , and two additional values, differing from the central one by $\approx 5\%$. Those curves can be compared with the difference between the cross section data and the computed NI component (open circles). The dot-dashed curves are empirical NI components, which will be discussed below. The following observations from the above comparison are not limited to the chosen examples, but hold quite generally:

a) Whether a QEP stands out in the data or not, in regions away from $x \approx 1, \sigma^{A,NE}$ is barely modified when α_n is changed by as much as 5% around some average value. Only in the immediate neighborhood of the QEP is $\sigma^{A,NE}$ sensitive to small variations in α_n .

b) In view of a), a precision extraction of $\sigma^{A,NE}$ in the region $x \approx 1$, and thus indirectly of α_n , requires a well-determined, locally small, inelastic background. The accuracy of such an extraction is limited by the precision in the input nucleon SF, the quality of data and of the calculated $f^{PN,A}$.

We summarize expectations for inclusive cross sections [1]:

i) On the low- ν , elastic side side of the QE region, cross sections for small Q^2 are predominantly NE and the quality of the extracted α_n depends on the precision with which one can calculate the point-nucleon nuclear SF $f^{PN,A}$ in the small wings, away from the peak.

ii) Approaching the QE region, NE components still dominate, provided Q^2 is not too large. If $f^{PN,A}$ is sharply peaked, as is the case for the lightest nuclei, the same will be observed in $\sigma^{A,exp} \approx \sigma^{A,NE}$. No matter what the kinematic conditions are, the QE region close to $x \approx 1$ is most sensitive to α_n and is therefore the primary source for the looked-for information.

iii) On the inelastic, large- ν side of the QE region, NE components decrease relatively to the increasing inelastic background.

iv) For further increasing ν , inclusive excitation of N resonances produces pseudo-resonances in the target. For $f^{PN,A}$ with a sharp maximum, pseudo-resonances in nuclei and genuine resonances in nucleons, peak at about the same x . For increasing Q^2 , pseudo-resonances gradually coalesce in a smooth background, due to overlapping tails of higher pseudo-resonances.

The extraction procedure follows from the above. First we define reduced cross sections on a p and a composite target A

$$K^{p,A}(E; \theta, \nu) = \frac{d^2 \sigma^{ep,eA}}{d\Omega d\nu} \bigg/ \sigma_M(E; \theta, \nu) = \left[\frac{F_2^{p,A}(x, Q^2)}{\nu} + \frac{2F_1^{p,A}(x, Q^2)}{M} \text{tg}^2(\theta/2) \right]. \quad (4.1)$$

Eqs. (2.7) and (2.8) show that $K^{A,NE}(x, Q^2)$ and $f^{PN,A}$ have a similar rapid variation with x .

Next we subtract the computed NI background from the data over the entire measured $x(\nu)$ -range. We then search for a continuous x range for which the difference of reduced cross sections $\Delta K^A \equiv K^{A,exp} - K^{A,NI}$ and $f^{PN,A}$ shows maximal similarity. In that range we identify

$$K^{A,exp} - K^{A,NI} \iff K^{A,NE} \quad (4.2)$$

and determine for each data-point in the selected x -range

$$\alpha_n(Q^2)|_{\mu_n} = \left[\frac{2MK^{A,NE}/w^A v^A - B^2/\eta}{1 + \text{tg}^2(\theta/2)/v^A} \bigg|_{x, Q^2} - [\alpha_p(Q^2)\mu_p]^2 \right]^{1/2} \quad (4.3)$$

$$= \left[2MR_T^{A,NE}/w^A \bigg|_{x, Q^2} - [\alpha_p(Q^2)\mu_p]^2 \right]^{1/2} \quad (4.4)$$

Above $w^A(x, Q^2) = f^{PN,A}(x, Q^2)G_d^2(Q^2)$; $v^A(x, Q^2) = x^2 C_{22}^A(x, Q^2)/[2(1 + \eta)]$ and $B^2(Q^2) = 2[G_E^N(Q^2)]^2/G_d^2(Q^2)$.

We remark that Eq. (2.4) also predicts that $K^{A,NE}$ and $f^{PN,A}$ have practically the same A -dependence. Eqs. (4.3), (4.4) show that residual dependence of $K^{A,NE}$ on both A and x is far weaker than the same in $f^{PN,A}$. In addition one notices in Eq. (4.3) a dependence on θ . For very forward scattering angles the above extraction method may occasionally become unstable. An example will be mentioned below.

Strict fulfillment of the above requirement implies that α_n is independent of the data points, which have been selected for the extraction. In practice one deals with data for fixed E, θ and varying x , hence with Q^2 varying over the measured ν -range. In general that variation is mild, but not insignificant for $Q^2 \lesssim 0.7 - 0.8 \text{ GeV}^2$, and the extracted α_n will vary there with Q^2 . But even for data sets with fixed Q^2 , experimental inaccuracies and the imperfections in the theoretical model, cause extracted α_n to depend on the selected data points x_j . Ultimately one has for each data set to determine an average $\langle \alpha_n \rangle$.

It is virtually impossible to incorporate in the analysis all experimental errors and uncertainties in both input and theory, and we therefore limit ourselves to the following:

a) Published tabulated cross sections give statistical and occasionally systematic errors, but frequently only the former are shown in figures. Only those are incorporated in our analysis. Most abundant and accurate are D data, and occasionally one can assign practically constant relative errors for selected x -intervals.

b) As mentioned in the Introduction the issue of the proton form factors is not yet settled. Two-photon exchange contributions to ep inclusive scattering apparently influence on the few % level [13, 14]. Although the E/M ratio for the proton as measured in the polarization transfer measurement [11, 12] is believed to be correct, p FFs, cannot be determined, without first to apply the above corrections to cross section data. This has not yet been done. The above reflects on both the proton data and the parametrization of Ref. [39] for α_n , which we used in Eqs. (4.3), (4.4).

At this point we remark that two-photon exchange contributions cannot be accommodated in a single generalized convolution (2.4). The observation, that data for $K^{exp}(x) - K^{NI}(x)$ and $f^{PN,A}(x)$ have very similar variation with x , does not allow more than a few % two-photon exchange contributions.

We therefore stuck to the procedure followed in Ref. [1], using two sets of proton FFs: one using the Jones results and a second one suggested in Ref. [36], both not yet corrected for two-photon exchange contributions. We expect the two methods to provide extremes between which the correct results will ultimately fall. For both sets we applied the error analysis a).

c) The uncertainty in the electric form factor of the neutron appears to be of no consequence. Assuming that the different parametrizations may be extrapolated to the largest Q^2 needed, the ratio $[G_E^n/G_E^p]^2$ in B^2 , Eq. (4.3) may vary by as much as 30%. However, for $Q^2 \gtrsim 0.5 \text{ GeV}^2$ the above B^2 term is far smaller than the first term in the numerator in Eq. (4.3), and its inclusion affects α_n by less than 1%!

We conclude this Section by the following remark. Our extraction method for $\langle \alpha_n \rangle$ rests on a test, checking whether the difference $K^{A,NE} = K^{A,exp} - K^{A,NI}$ and the SF $f^{PN,A}$ have similar x -dependence over a continuous set of data points. Having determined from those values $\alpha_n(x_i)$ and their average $\langle \alpha_n \rangle$, we calculate the corresponding NE component $NE(\langle \alpha_n \rangle) \equiv \sigma^{A,NE}(\langle \alpha_n \rangle)$. Likewise NI(comp) stands for the computed $\sigma^{A,NI}$.

The above defined $NE(\langle \alpha_n \rangle)$ are constructed to fit in the mean $NE(\text{extr}) = \text{data} - NI(\text{comp})$ in the selected range of data points x_i around the QEP. Those actually continues to approximately reproduce $NE(\text{extr})$ over a range beyond the chosen points of extraction.

Barring the effect of a mildly varying Q^2 over the the points of a data set, perfect data and an exact theory for NI ought to produce a $NE(\langle \alpha_n \rangle)$, fitting $NE(\text{extr})$ over the *entire* x or ν interval. In the following Section we shall find that deviations set in beyond some ν , where NI about overtakes NE. Those deviations reach a maximum around the position of the first pseudo-resonance and then rapidly decreases to 0. The culprit may well be NI(comp), in which case we define an empirical NI by

$$NI(\text{emp}) \approx \text{data} - NE(\langle \alpha_n \rangle) \quad (4.5)$$

By construction $NE(\langle \alpha_n \rangle)$ closely fits $\text{data} - NI(\text{emp})$. We shall return to a possible source of the apparent insufficiency of NI(comp).

V. DATA AND RESULTS.

Below we report on $\alpha_n(G_M^n)$, extracted from abundant cross sections for total inclusive scattering of unpolarized electrons on D and ^4He . Additional information comes from, partly re-analyzed sparse data on their transverse components for both targets.

We start with particulars on data and results collected in Table I. Columns refer to target, beam energy, scattering angle, range of x, Q^2 and the value $\bar{Q}^2 \equiv Q^2(\nu_{QEP})$ at the QEP. In the last column we first mention the number of selected data points x_j for each data set. Those are followed by the weighted averages of the extracted α_n with their

error of the mean, which includes statistical errors on the cross sections for both parameterizations I and II discussed in Section III. Since systematic errors have been disregarded, the stated error bars should be considered as lower limits.

Only a sample of analyzed data sets are presented in Figs. 1-12. The two options I, II for p FFS produce the same elastic ep cross sections with different E/M ratios. For that reason there is no need to specify the option in Figs.: it enters only in the ultimately extracted α_n .

HE1): $E = 2.02 \text{ GeV}, \theta = 20^\circ; E = 3.595 \text{ GeV}, \theta = 16, 20^\circ; \bar{Q}^2 = 0.434, 0.873, 1.270 \text{ GeV}^2$ [4].

The above NE3 data have previously been analyzed [1] and the very good fits on the elastic side of the QEP have been attributed to accurate knowledge of the required density matrices and the inclusion of C_{22} . The present refined calculations produce the observed rise of the first two cross sections towards the pseudo-resonances. Those are locally $\approx 20\%$ short of the first two data sets and $\approx 10\%$ for the third one. Fig. 3 illustrates the latter one. Since the involved Q^2 are relatively small, FFs for both options I, II are essentially the same.

HE2): $E = 2.7, 3.3, 3.6, 3.9, 4.3 \text{ GeV}, \theta = 15^\circ, \bar{Q}^2 = 0.453, 0.662, 0.781, 0.907, 1.090 \text{ GeV}^2; E = 0.9, 1.1 \text{ GeV}, \theta = 85^\circ, \bar{Q}^2 = 0.78, 1.09 \text{ GeV}^2$. [2, 3].

The above NE9 cross section data are unpublished parts of the PhD. Thesis of J-P Chen [2]. Those are in principle a welcome source of information on α_n over a dense Q^2 -range, which partly overlap the Q^2 range of the the NE3 data, but extend beyond the QEP and the adjacent minimum, and occasionally into the pseudo-resonance region.

A comparison with data, illustrated by Fig. 4 for $E = 4.3 \text{ GeV}, \theta = 15^\circ$ shows a pattern, similar to that for the NE3 data. There is a deficiency of $\approx 30\%$ at the peak of the first pseudo-resonance for the set with lowest Q^2 , which is reduced to $\approx 10\%$ for the larger Q^2 .

HE3): $R_{L,T}$ for approximately constant $|q| = 1.05$ and running ν [2, 3].

Eq. (4.4), using R_L is a simpler expression than Eq. (4.3), for reduced, total inclusive cross sections and requires only additional knowledge of α_p . Extracted α_n from, in principle favored R_T data, ought to be close to the ones from cross section data HE2) with approximately the same Q^2 , yet Table I shows fairly large deviations. The following may well be one of the causes.

In order to be eligible as partners for a Rosenbluth extraction, some data sets HE2) have been chosen for fixed $\theta = 85^\circ$ and at two beam energies, such that the x, Q^2 *approximately* coincide with those of the first set with $\theta = 15^\circ$ at different beam energies. Since such a match is never perfect, extrapolations of data are necessary.

R_T is relatively large for $x \approx 1$, but that is also region where the point-nucleon SF $f^{PN,A}(x, Q^2)$ varies sharply with x . A 3% error or uncertainty in an extrapolation of data points to values for $x \approx 1$, may cause a 10% change in $f^{PN,A}$ on which $F_2^{A,NE}$ depends linearly. We thus tend to actually trust more the involved total cross section information. A PWIA analysis of R_T is reported to be in good agreement with data on the elastic side of the QEP [45].

The following D data sets are nearly all for appreciably larger Q^2 than for He.

D1): $E = 4.045 \text{ GeV}; \theta = 15, 23, 30, 37, 45, 55^\circ; \bar{Q}^2 = 0.972, 1.940, 2.774, 3.535, 4.251, 4.900 \text{ GeV}^2$ [46, 47].

In our previous analysis we searched for cross section data dominated by F_2^p . This limited the suitable data to the two lowest θ sets above [1]. With reliable parameterizations for both $F_{1,2}^p$, the above restriction is lifted, providing a far larger number of data points for analysis.

Only in the data for the lowest two angles is a pseudo-resonance clearly visible: For $\theta \geq 30^\circ$ the pseudo-resonance structure gradually disappears. One still notices a minimum beyond the QEP, but for further growing Q^2 , there remains no more than a break in the slope of $\ln(\sigma)$. The agreement over the entire range of ν , with the exception of the intermediate range, discussed at the end of Section IV, is good and sometimes excellent. It comprises qualitatively different features, as are the position and intensity at the minimum between the QEP and the pseudo-resonance, as well as the position of the peak of the pseudo-resonance. In those regions the NI components first compete with NE, overtake those and finally dominate.

An underestimate of the computed NI in the intermediate ν -range, and its remarkably similar relative size is apparent in virtually all analyses. For example, Figs. 5, 2 and 6 for $\theta = 15, 30, 55^\circ$ show a bell-shaped excess over NE(extr) on the inelastic side of the QEP, as extracted from Eqs. (2.1), (2.7), (2.8). Dot-dashes show NI(emp), which produce NE($\langle\alpha_n\rangle$) for all ν .

D2): $E = 5.507 \text{ GeV}, \theta = 15.15, 18.98, 22.81, 26.82^\circ; \bar{Q}^2 = 1.75, 2.50, 3.25, 4.00 \text{ GeV}^2$ [5, 48].

The kinematics of the above NE11 data partly overlap those of D1). Virtually all remarks on D1) hold also for D2) (cf. Figs. 7,8 for $\theta = 15.15, 26.81^\circ$.)

D3): R_T for the x, Q^2 kinematics of D2 [48].

For kinematics close to those in D2), the extracted α_n from R_T are comparable or slightly higher than from D2). Otherwise much the same remarks as for HE3) above hold also here: In order to obtain x, Q^2 matching for a Rosenbluth separation, the unavoidable handling of data around the QEP $x \approx 1$ is bound to be imprecise in view of the sensitivity of $f^{PN,D}$ around the QEP, which grows with Q^2 .

D4): $E = 2.015 \text{ GeV}, \theta = 38.84^\circ; E = 3.8 \text{ GeV}, \theta = 47.86^\circ; E = 4.212 \text{ GeV}, \theta = 53.39^\circ; E = 5.12 \text{ GeV}, \theta = 56.64^\circ. \bar{Q}^2 = 1.22, 3.15, 5.10, 6.83 \text{ GeV}^2$ [49]

The above NE18 SLAC data for D are for high E and relatively large θ and are restricted to the immediate QE region. In spite of considerable experimental noise, those data are of interest, in view of the large Q^2 involved. Computed results are in agreement with data around the QEP, which show much scatter. Beyond that region, disagreements are less than $\approx 25\%$ (cf. Fig. 9). For reasons already mentioned we did not analyze parallel data for heavier targets.

D5): $E = 9.744, 12.565, 15.730, 17.301, 18.476, 20.999$ GeV, $\theta = 10^\circ$. $\bar{Q}^2 = 2.5, 4.0, 6.0, 7.1, 8.0, 10.0$ GeV² [50].

Cross sections computed with rather primitive input show on a tight logarithmic scale reasonable agreement with the above old data, but on a linear scale considerable scatter in data is apparent. The above Rock data for small θ provide a unique example of marginal stability: the $E = 9.744$ provide two adjacent subsets with rather different average for α_n . Both cause $\langle\alpha_n\rangle$ to have relatively large error bars (Table I).

The main interest is their values out to the largest Q^2 , measured until this date. Figs. 10-12 show results for $E = 15.73, 18.476, 20.999$ GeV. Table I shows that for $E = 18.476$ $\langle\alpha_n\rangle$ is relatively large, and not in line with other $\langle\alpha_n\rangle$ in the data set. One observes close correspondence between $\langle\alpha_n\rangle$, extracted from different data sets.

The overall outcome is compiled in Figs. 13-15. In inserts we give symbols for experiments (empty ones for older and filled symbols for re-analyzed ones), kind of data and Ref. numbers. Fig. 13 contains results from He data, which are all for low $Q^2 \leq 1.3$ GeV² with α_n , close to 1. For those Q^2 , differences for the choices I, II are relatively small (see Table I); displayed results are for I. In detail:

- i) Asymmetry measurements in QE $^3\text{He}(\vec{e}, e')$ [51, 52, 53].
- ii) Preliminary results of the analysis of i), without 3-body channels in the FSI [54].
- iii) Ratios of exclusive D break-up cross sections, with p , respectively n detected [55, 56, 57] (In view of the criticism of Jourdan *et al.* [58], we omit some old data [59]).
- iv) The above HE1)-HE3) [2, 3, 4] $^3\text{He}(\vec{e}, e')$.

Fig. 14 contains results, extracted from the sets D1)-D5) with $Q^2 \geq 1.0$ GeV² [5, 46, 47, 48, 49, 50]. The only displayed result of a previous analysis is D2) [48]. Fig. 15 is the same as Fig. 14 for choice II of FFs.

In both the drawn lines are inverse polynomial fits of $\alpha_n(\bar{Q}^2)$ from the D data, as used in Ref. [36]

$$\begin{aligned}\alpha_n(\bar{Q}^2)^I &= 1/[1 + 0.007437\bar{Q}^2 + 0.002815161\bar{Q}^4 - 0.000115008\bar{Q}^6] \\ \alpha_n(\bar{Q}^2)^{II} &= 1/[1 + 0.06568\bar{Q}^2 - 0.00678662\bar{Q}^4 + 0.000323355\bar{Q}^6]\end{aligned}\quad (5.1)$$

Although only approximately valid for $\bar{Q}^2 \geq 1.5$ GeV², the fits extrapolate to the 'correct' $\alpha_n(0) = 1$. In spite of scatter in the data two observations on $\langle\alpha_n\rangle$ stand out:

- a) $\alpha_n(\bar{Q}^2)$ clearly decreases with increasing Q^2
- b) There is close correspondence between extracted values from different data sets, for instance for $\bar{Q}^2 = 2.5, 4.0, \approx 7.0$ GeV².

VI. SUMMARY AND CONCLUSIONS.

The overwhelming majority of its properties cannot be measured on free neutrons and one is therefore led to study those on neutrons, which are bound in nuclear targets. The extraction of any such property thus demands an accurate treatment of the embedding of the neutron in that target. Even when feasible, one has in addition to assume, that those extracted quantities are the same as for a neutron in vacuum, i.e. that the former are not *intrinsically* modified by the medium. Nowadays one can accurately compute nuclear properties for $A \leq 4$, and there seems to be no evidence for medium effects. Those may well be artifacts of approximations.

The present contribution deals with the extraction of the reduced magnetic form factor of the neutron from cross sections for the inclusive scattering of electrons from the lightest targets.

Part of the available data have been analyzed before [1]. There we limited ourselves to those kinematic parts of data sets, where the elastic absorption of an exchanged photon on a nucleon had been estimated to be much in excess of the inelastic ones, which were subsequently disregarded: That procedure not only affected accuracy. It also limited the analysis to the immediate neighborhood of QE peaks, where the NI background is very small. That region covers only a small section of the data, which generally stretch over wide energy-loss ranges.

Ref. [1] followed the principal ideas of Lung [48] and of older work, using rather primitive tools and input[50]. A number of incentives called for a re-analysis of the above results. Together with our wish to include the above mentioned neglected kinematic areas, we included previously disregarded data. We used moreover recently published, precise parameterizations of the input SF $F_{1,2}^p$ for the proton, valid through resonances and reaching into the DIS region. For medium and large Q^2 those parametrizations become unreliable and we had to fall back on parameterizations of resonance-averaged F_2^p . In addition, it appeared possible to up-date the input for the determination of

the additionally required neutron SF. Finally we could also sharpen some theoretical tools. As a result the present analysis constitutes a significant refinement of the previous one.

The above comprehensive theory for the extraction of the magnetic form factor of the neutron G_M^n addressed relatively abundant total cross for inclusive electron scattering, and scarce data on their transverse components. In principle several targets are accessible to an analysis, but only for the lightest nuclei can one presently calculate with great precision nuclear information, which describes the above embedding. Most of the available data on D are of good quality and contain several data sets covering a range of partly overlapping Q^2 . The latter fact enables desirable consistency checks. For ${}^4\text{He}$ there are only available rather old, low- Q^2 data of lesser quality and for which also the theory is less accurate than for higher Q^2 . Nevertheless we analyzed all.

The cornerstone of our analysis is the possibility to reliably compute components of the nuclear inclusive cross sections, due to inelastic virtual photon absorption on nucleons, provided F_k^N are known. Those nuclear NI processes dominate virtually all kinematic regions, except the ones around the QE peak, where elastic absorption of virtual photons on nucleons competes with inelastic processes.

Cross sections in those QE regions contain the desired information on form factors, and their isolation is therefore of primary importance. Simple theoretical considerations predicts the same x -dependence of the NE components of cross sections and the calculable Structure Function $f^{PN,A}(x, Q^2)$ of a fictitious target, composed of point-nucleons. The latter drops sharply from its QE peak at $x \approx 1$: in the case of a D by a factor $\approx 10 - 50$.

One thus compares the functional dependence on x of the above difference with the same for $f^{PN,A}(x, Q^2)$. In regions where close similarity is found, one identifies that difference with the desired NE components of cross sections.

For all data sets, the above differences between measured reduced total cross sections and calculable inelastic backgrounds, appear to follow the predicted x -behaviour, roughly for $x \gtrsim 0.7 - 0.8$. The above provides incontrovertible proof that in the above restricted areas, where the x -dependence is most outspoken, the above defined differences are indeed the NE components of the cross sections.

For each data set we then selected a continuous x -range, for which the correspondence with the x -dependence of $f^{PN,A}$ is best. Dependent on the quality of the data set, the number of thus selected x points may be as large as 17. Ideally, those should reproduce G_M^n , independent of x or A .

We first summarize our results:

A) There is similarity and sometimes reasonable correspondence between the extracted α_n from different targets. Differences may in part be due to the same in the quality of the older low Q^2 , He data and the more recent D experiments. It is in particular satisfactory that the high-quality $E = 4.045$ and $E = 5.507$ D data yield corresponding $\alpha_n(Q^2)$ for similar Q^2 . The same is the case, if the old data of Rock *et al.* are included.

B) Our results confirm and reinforce an important conclusion already reached in our previous analysis: α_n from D data seems to fall faster with Q^2 than the older Lung results indicate. The same is the case for the slope of the older He data, but as stated above, we have reservations regarding the used parametrization for F_2^p for the lowest Q^2 and the quality of the data. For growing Q^2 , the NE3 and NE9 ${}^4\text{He}$ data and the average behavior of the D data for corresponding Q^2 produce similar α_n .

We have emphasized the identification of $\sigma^{A,NE}$ over finite x -ranges. On the inelastic side of the QEP for virtually all D data sets, the use of NI, computed with the recent parametrization of F_2^p , produces deviations from NE components, computed with $\langle \alpha_n \rangle$. Those roughly start where $\text{NE} \approx \text{NI}$, and grow to a 10-15 % under-estimate towards the peak of the pseudo-resonance position, beyond which the discrepancy rapidly disappears. An increase of the NI background of just the above size extends the above local fit of the computed NE cross section to comprise the entire ν -range.

The discrepancy may be the result of a relatively modest under-estimate of the transition strength for inclusive excitation of the first resonance for larger Q^2 . It would effect mostly the low ν tail of NI, because more inelastic parts are screened by overlapping resonances. We emphasized that one cannot apply an ad hoc change of one parameter in a multi-parameter fit of F_2^p .

In spite of the manifestly succesful local isolation of elastic components of the inclusive cross sections, the actual extraction of G_M^n from those is not straightforward. We mention a few sources which may influence the precision of the extraction:

1) Disregarding experimental accuracies, the test of the central requirement is optimal when the inelastic background is a small fraction of the total cross section. The latter is the case in the immediate neighborhood of the QEP, where the elastic components are most sensitive to variations of G_M^n . The small values of the inelastic background there are due to the tails of overlapping resonances, which by nature have least accuracy. Consequently, changes in a very small background around the QEP may have 1% effects on the extracted α_n .

2) Total inclusive cross sections contain in principle Meson Exchange Contributions (MEC), which should be eliminated from the data, before those are manipulated as described. Little is known of MEC contributions for high- Q^2 inclusive processes. As a measure of their size we suggested recent results for the exclusive processes ${}^3\text{He}(\text{e}, \text{e}'\text{p})\text{D}$ and ${}^4\text{He}(\text{e}, \text{e}'\text{p}){}^3\text{He}$. Polarization variables appear sizeably affected by MEC, but only tiny corrections are reported on cross sections for inclusive scattering with unpolarized beams [61].

3) Present uncertainties regarding the proton form factors.

The above concludes our program to extract G_M^n from data on inclusive cross sections. We are well aware that our method is an indirect one, which forced us to make careful checks on intermediate steps. Those unfortunately could not circumvent present uncertainties in input. At least the unknown behavior of G_E^n for large Q^2 seems not to be of relevance. Unless the unknown G_E^n for larger Q^2 will turn out to deviate strongly from assumed extrapolations from low Q^2 , its influence will remain negligible.

The above clearly demonstrates that the described extraction method is a realistic and internally consistent one. We do not think that theoretical tools can be much improved, but it is highly desirable to eliminate uncertainties in some input elements of the calculations. In parallel new inclusive scattering data on ^3He and ^4He could add information and furnish further proof of consistency.

In the meantime we are looking forward to final results for G_M^n from the $D(e, e'p)X/D(e, e'n)X$ experiment of Brooks *et al.* Preliminary results seem to yield a smaller slope for α_n than in Figs. 14,15 [62].

VII. ACKNOWLEDGMENTS.

ASR is much indebted to Cynthia Keppel, Eric Christy and John Arrington for generously making available parameterizations of proton structure functions, prior to publication and J.A. for having added relevant comments. He is grateful to J-P. Chen, who provided unpublished experimental material, simultaneously making persistent and correct critical remarks on the role of the NI background.

-
- [1] A.S. Rinat, M.F. Taragin and M. Viviani, Phys. Rev. C 70, 014003 (2004)
 - [2] J.P. Chen, PhD Thesis, Stanford Univ. 1992.
 - [3] Z.-E. Meziani, *et al.*, Phys. Rev. Lett. 69, 41 (1992).
 - [4] D.B. Day *et al.*, Phys. Rev. C 48, 1849 (1993).
 - [5] L.M. Stuart *et al.*, Phys. Rev. D 58, 032003 (1998).
 - [6] Y. Liang *et al.*, [arXiv:nuc1-exp/0410027]; M.E. Christy, private communication. See also hallcweb.jlab.org/resdata
 - [7] M. Osipenko *et al.*, Phys. Rev. D 67, 092001 (2003).
 - [8] A.S. Rinat and M.F. Taragin, Phys. Lett. B 551, 284 (2003).
 - [9] J. Arrington, Phys. Rev. C 68, 034325 (2003).
 - [10] J. Arrington, Phys. Rev. C 69, 022201 (2004).
 - [11] M. Jones *et al.*, Phys. Rev. Lett. 84, 1398 (2000); Third Workshop on 'Perspective in Hadronic Physics, Trieste 2001, IT; to be published;
 - [12] M. Jones *et al.*, Phys. Rev. Lett. 88, 092301 (2002).
 - [13] P.A.M. Guichon and M. Vanderhaegen, Phys. Rev. Lett. 91, 142303 (2003); P.G. Blunden, W. Melnitchouk, and J.A. Tjon, *ibid.*, 91, 142304 (2003); Y.C. Chen *et al.*, [arXiv:hep-ph/0403058].
 - [14] W. Melnitchouk, private communication.
 - [15] S.A. Gurvitz and A.S. Rinat, Progress in Nuclear and Particle Physics, Vol. 34, 245 (1995).
 - [16] S.A. Gurvitz and A.S. Rinat, Phys. Rev. C 65, 024310 (2002).
 - [17] H. Gersch, L.J. Rodriguez, and Phil N. Smith, Phys. Rev. A 5, 1347 (1973).
 - [18] A.S. Rinat and M.F. Taragin, Phys. Rev. C 60, 044001 (1999); *ibid.*, C 62, 034602 (2000).
 - [19] R. L. Jaffe, Proceedings Los Alamos Summer School, 1985; Ed. M. Johnson, A. Picklesimer (Wiley; NY, 1986).
 - [20] G.B. West, Interactions between Particles and Nuclear Physics. Ed. R.E. Mischke, AIP (NY 1984), p.360.
 - [21] A.S. Rinat and M.F. Taragin, in preparation.
 - [22] A.S. Rinat and M.F. Taragin, [arXiv:nuc1-th/0501006].
 - [23] G.B. West, Ann. of Phys. (NY) 74, 646 (1972); W.B. Atwood and G.B. West, Phys. Rev. D 7, 773 (1973).
 - [24] M.M. Sargassian, S. Simula and M.I. Strikman, Phys. Rev. C 66, 024001 (2002).
 - [25] C.H. Llewellyn Smith, Phys. Lett. B128, 107 (1983); M. Ericson and A.W. Thomas, *ibid.*, B128, 112 (1983).
 - [26] S. Mandelstam, Proc. Royal Soc. A 244, 491 (1958).
 - [27] M.M. Hoenig and A.S. Rinat, Phys. Rev. C 18, 2683 (1978).
 - [28] A.S. Rinat and M.F. Taragin, Phys. Rev. C 65, 042201(R) (2001).
 - [29] M. Viviani, A. Kievsky, and A.S. Rinat, Phys. Rev. C 67, 034003 (2003).
 - [30] A.S. Rinat and M.F. Taragin, Nucl. Phys. A598, 349 (1996); *ibid.*, A620, 412 (1997); Erratum: *ibid.*, A623, 773 (1997); Phys. Rev. C 60, 044601 (1999).
 - [31] M. Arneodo *et al.*, Phys. Lett. B 364, 107 (1995); P. Amadraz *et al.*, Phys. Lett. B 295.
 - [32] A. Bodek and J.L. Ritchie, Phys. Rev. D 23, 1070 (1981).
 - [33] E.D. Bloom and F.J. Gilman, Phys. Rev. 25, 1140 (1970); Phys. Rev. D 4, 2901 (1971).
 - [34] I. Niculescu *et al.*, Phys. Rev. Lett. 85, 1182, 1186 (2000).

- [35] W. Melnitchouk, Phys. Rev. Lett. 86, 35 (2001).
- [36] H. Budd, A. Bodek, and J. Arrington, [[arXiv:hep-ex/0308005](#)].
- [37] J. Arrington, [[arXiv:nucl-ex/0312017](#)].
- [38] I.A. Qattan *et al.*, Phys. Rev. Lett. 94, 142301 (2005)
- [39] E. Brash, A. Kozlov, Sh. Li, and G.M. Huber, Phys. Rev. C 65, 051001 (2002).
- [40] J. Bermuth *et al.*, Phys. Lett. B564, 199 (2003).
- [41] S. Galster *et al.*, Nucl. Phys. B32, 221 (1971).
- [42] R. Schiavilla and I. Sick, Phys. Rev. C 64, 041002(R) (2001).
- [43] A.F. Krutov and V.E. Troitsky, Eur. Phys. J. A16, 285 (2003).
- [44] R. Madey *et al.*, Phys. Rev. Lett, 91, 122002 (2003); G. Warren *et al.*, Phys. Rev. Lett, 92, 042301 (2004).
- [45] C. Ciofi degli Atti, private communication to J-P Chen, cited in Ref. [3].
- [46] I. Niculescu *et al.*, Phys. Rev. Lett. 85, 1182 (2000).
- [47] J. Arrington *et al.*, Phys. Rev. C 64, 014602 (2001).
- [48] A. Lung *et al.*, Phys. Rev. Lett 70, 718 (1993); PhD. thesis, The American University, Washington D.C. 1992.
- [49] J. Arrington *et al.*, Phys. Rev. C 53, 2248 (1996).
- [50] S. Rock, *et al.*, Phys. Rev. Lett. 49, 1139 (1982); Phys. Rev. D 46, 24 (1992).
- [51] H. Gao *et al.*, Phys. Rev. C 50, R546 (1994); Nucl. Phys. A 632, 170c (1998).
- [52] W. Xu *et al.*, Phys. Rev. Lett. 85, 2900 (2000); F. Xiong *et al.*, *ibid.*, 87, 242501 (2001).
- [53] W. Xu *et al.*, Phys. Rev. C 67 012201(R) (2003).
- [54] A. Kievsky, E. Pace, and G. Salme, Europ. Physics Journal A (supplement) 19, 87 (2004).
- [55] H. Anklin *et al.*, Phys. Lett. B 336, 313 (1994).
- [56] H. Anklin *et al.*, Phys. Lett. B 428, 248 (1998).
- [57] G. Kubon *et al.*, Phys. Lett. B 524, 26 (2002).
- [58] J. Jourdan, I. Sick, and J. Zhao, Phys. Rev. Lett. 79, 5186 (1997).
- [59] E.E.W. Bruins *et al.*, Phys. Rev. Lett. 75, 21 (1995).
- [60] R. Schiavilla *et al.*, Phys. Rev. Lett. 94, 072303 (2005).
- [61] R. Schiavilla *et al.*, Phys. Rev. C 72, 064003 (2005).
- [62] W. Brooks, private communication, Nucl. Phys. A 750, 261 (2005).

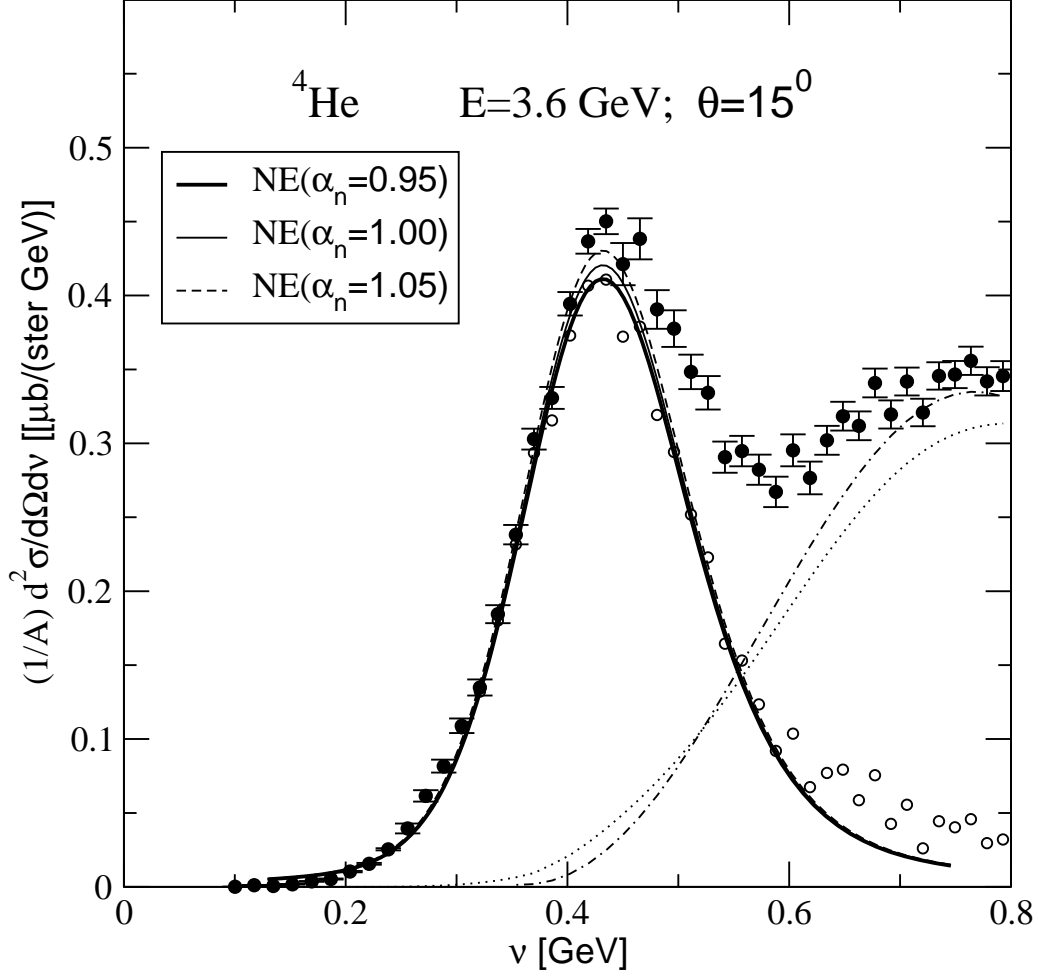


FIG. 1: Inclusive cross section on ${}^4\text{He}$ for $E = 3.6 \text{ GeV}$, $\theta = 15^\circ$, $\bar{Q}^2 = 0.781 \text{ GeV}^2$. Filled and empty circles represent SLAC NE9 data [3] with their statistical errors, respectively cross sections, from which the *theoretical* NI part (dotted curve) has been subtracted. Empty circles should carry error bars coming from the data and the NI part, but since we cannot at present estimate those, we have preferred not to show them. up to the last extraction point used. The difference is compared with $\sigma^{\text{He}, NE}$ for $\alpha_n = 1.00, 1.00 \pm 0.05$ (curves). Dot-dashes represent an NI(emp), defined as $\sigma^{\text{tot}} - \sigma^{NE}$.

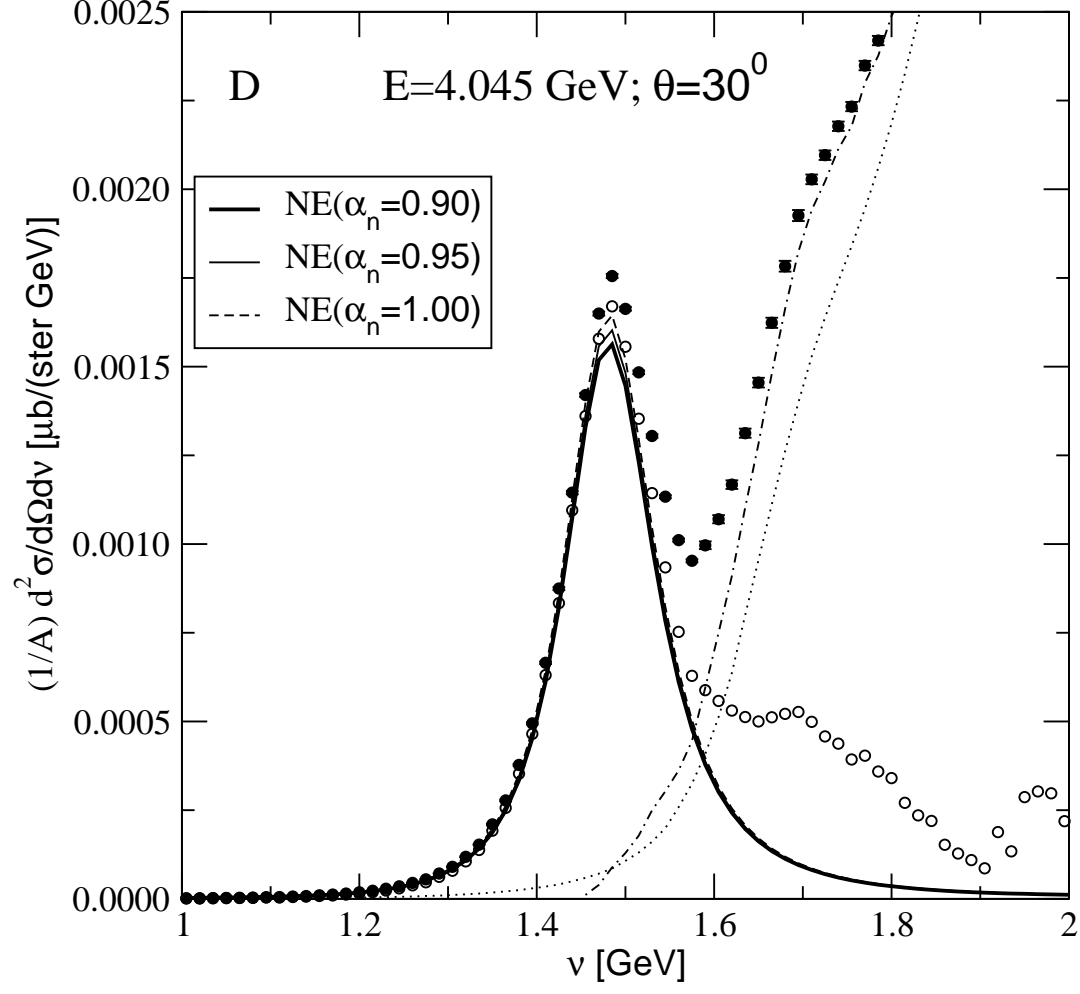


FIG. 2: As Fig. 1 for D at $E = 4.045 \text{ GeV}$, $\theta = 30^\circ$, $\bar{Q}^2 = 2.774 \text{ GeV}^2$. Data: Jlab E89-009 [46]. NE curves are for $\alpha_n = 0.95, 0.95 \pm 0.05$.

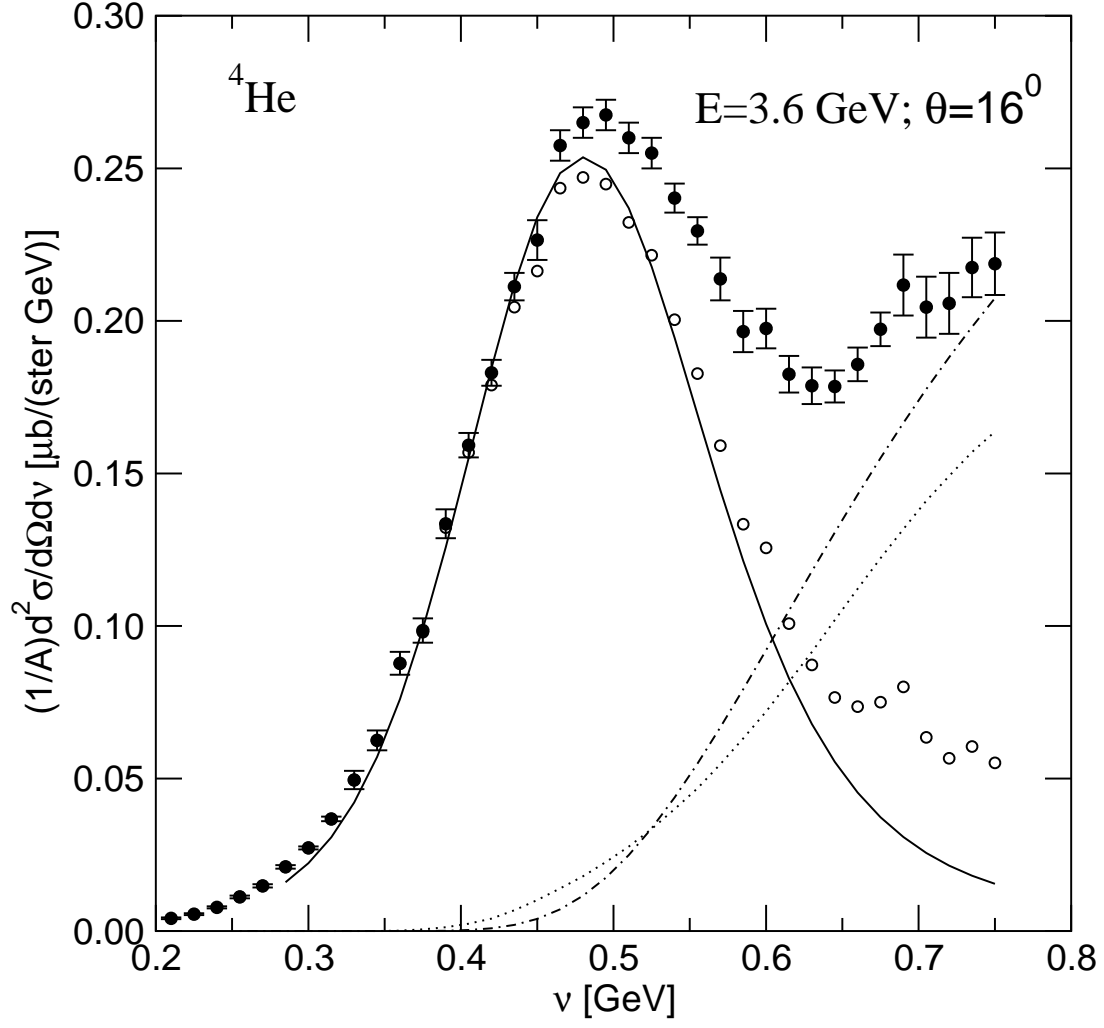


FIG. 3: As Fig. 1 for ${}^4\text{He}$ at $E = 3.595 \text{ GeV}$, $\theta = 16^\circ$. $\bar{Q}^2 = 0.873 \text{ GeV}^2$. Data: SLAC-Virginia NE3 [4]. NE curve for $\alpha_n = 1.006$.

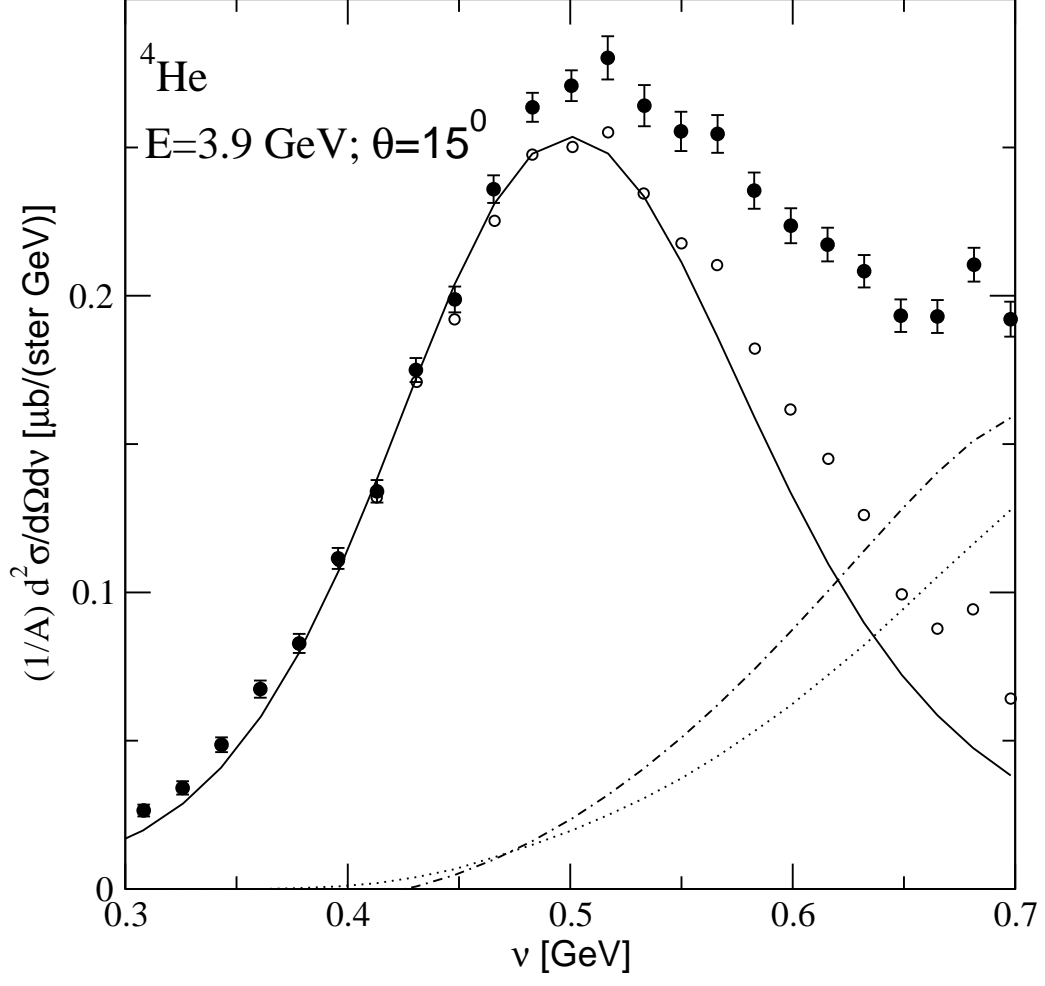


FIG. 4: As Fig. 1 for ${}^4\text{He}$ at $E = 3.9 \text{ GeV}$, $\theta = 15^\circ$, $\bar{Q}^2 = 0.907 \text{ GeV}^2$. Data: SLAC NE9 [3]. NE curve for $\alpha_n = 1.007$.

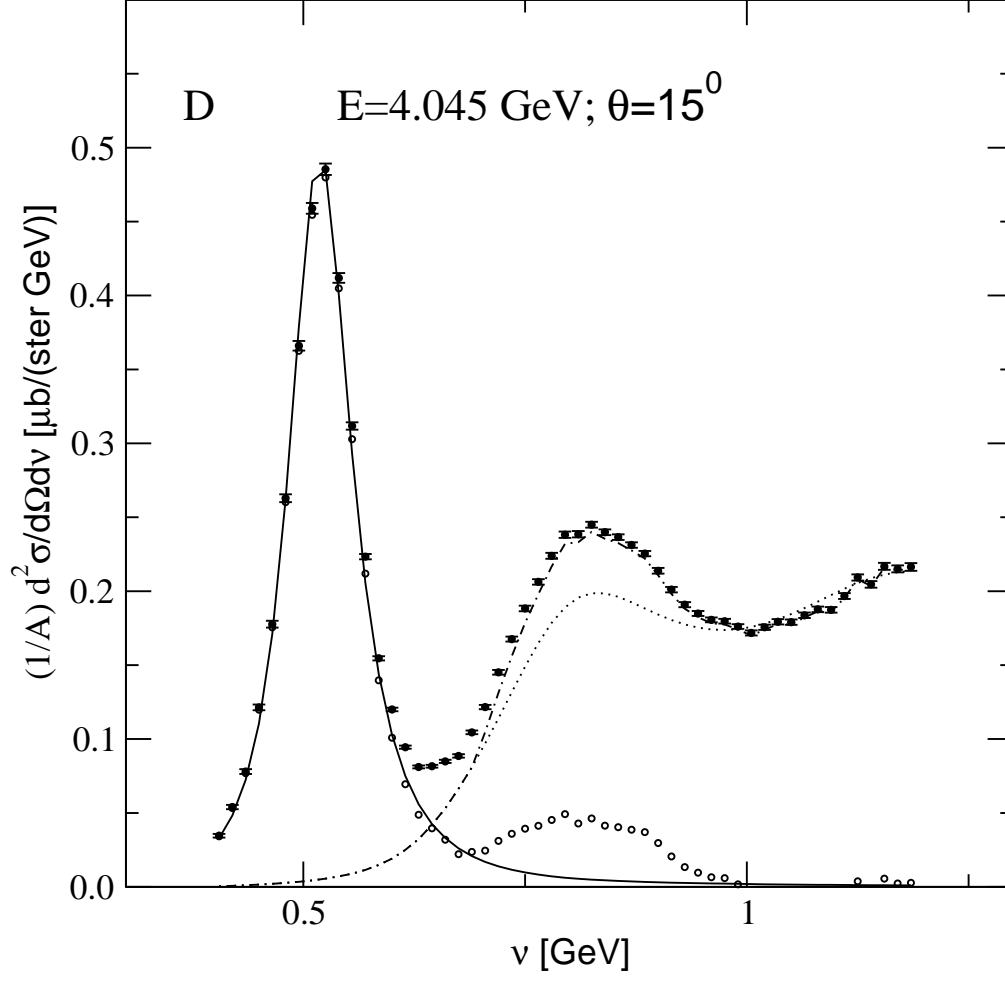


FIG. 5: As Fig. 1 for D at $E = 4.045 \text{ GeV}$, $\theta = 15^\circ$, $\bar{Q}^2 = 0.972 \text{ GeV}^2$. Data: JLab E89-009 [46, 47]. NE curve for $\alpha_n = 1.004$.

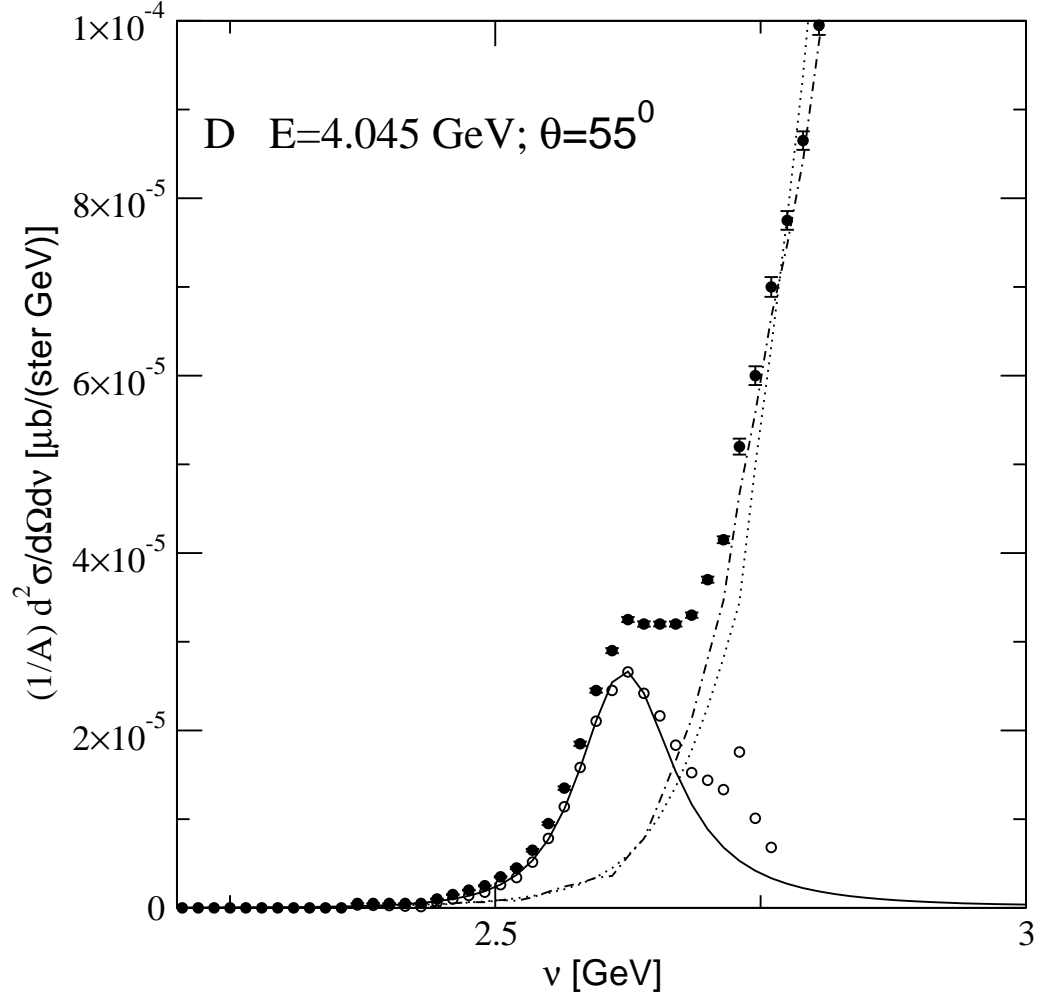


FIG. 6: As Fig. 1 for D at $E = 4.045$ GeV, $\theta = 55^\circ$, $\bar{Q}^2 = 4.900$ GeV². Data: JLab [46]. NE curve for $\alpha_n = 0.991$.

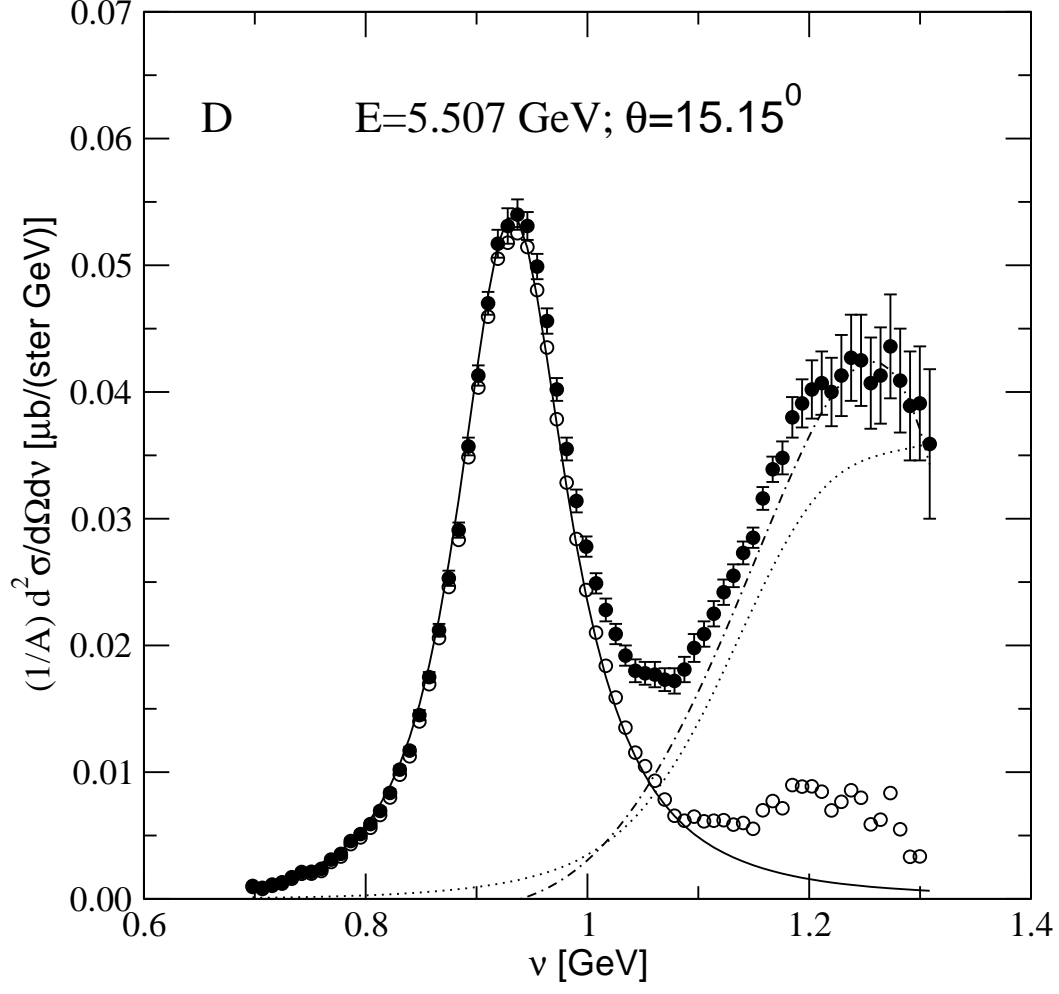


FIG. 7: As Fig. 1 for D at $E = 5.507 \text{ GeV}$, $\theta = 15.15^\circ$, $\bar{Q}^2 = 2.750 \text{ GeV}^2$. Data: SLAC NE11 [5]. NE curve for $\alpha_n = 1.008$.

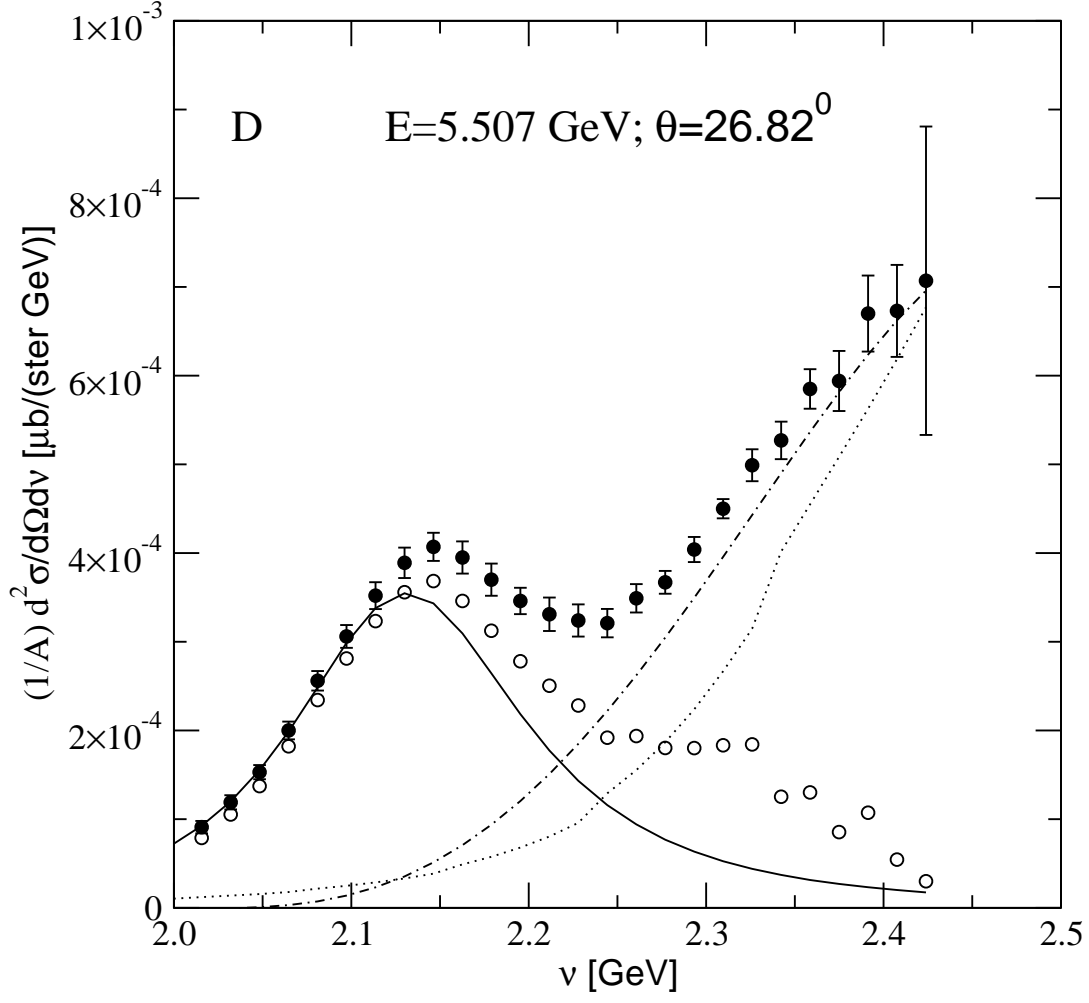


FIG. 8: As Fig. 1 for D at $E = 5.507 \text{ GeV}$, $\theta = 26.86^\circ$, $\bar{Q}^2 = 4.000 \text{ GeV}^2$. Data: SLAC NE11 [5]. NE curve for $\alpha_n = 0.951$.

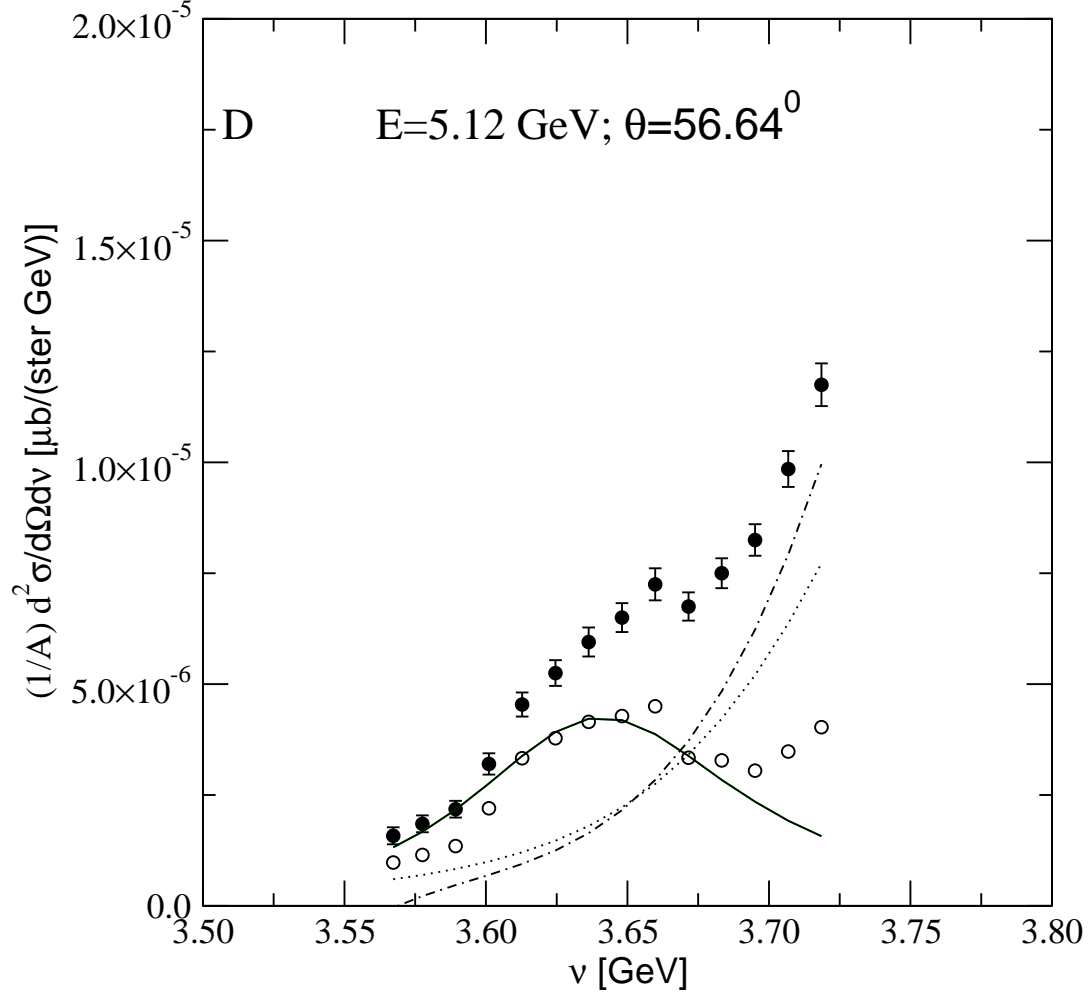


FIG. 9: As Fig. 1 for D at $E = 5.12 \text{ GeV}$, $\theta = 56.64^\circ$, $\bar{Q}^2 = 6.83 \text{ GeV}^2$. Data: SLAC NE18 [47]. NE curve for $\alpha_n = 0.842$.

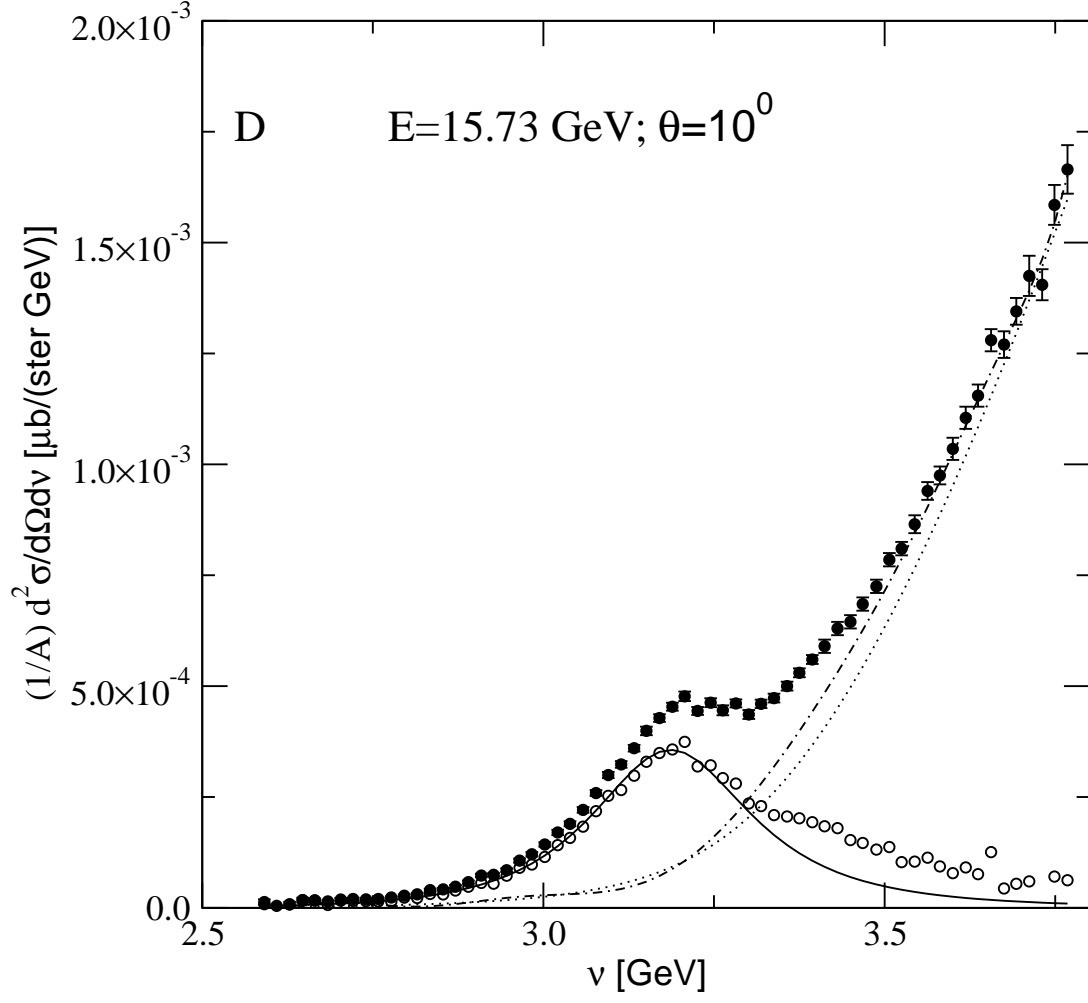


FIG. 10: As Fig. 1 for D at $E = 15.73 \text{ GeV}$, $\theta = 10^\circ$, $\bar{Q}^2 = 6.00 \text{ GeV}^2$. SLAC E133 data [50]. NE curve for $\alpha_n = 0.854$.

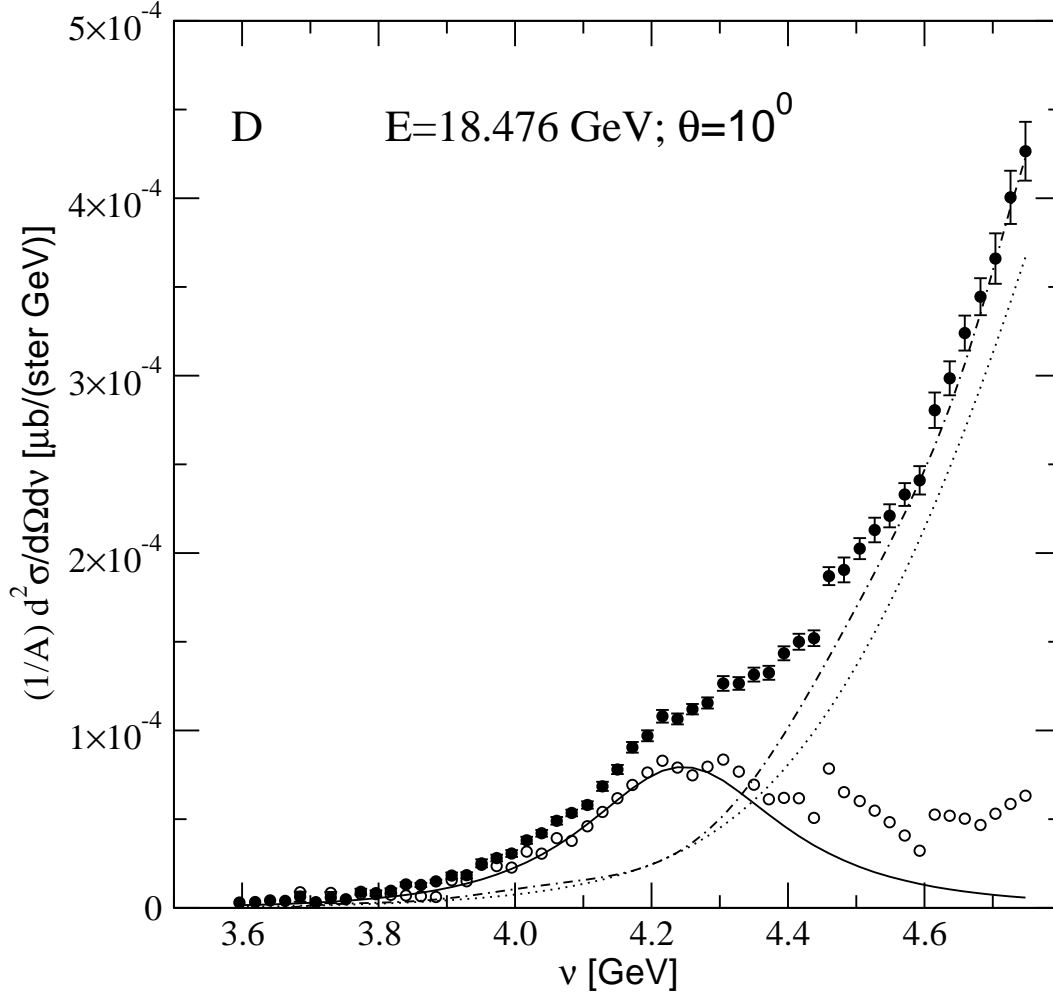


FIG. 11: As Fig. 1 for D at $E = 17.301 \text{ GeV}$, $\theta = 10^\circ$. $\bar{Q}^2 = 7.12 \text{ GeV}^2$. SLAC E133 data [50]. NE curve for $\alpha_n = 0.879$.

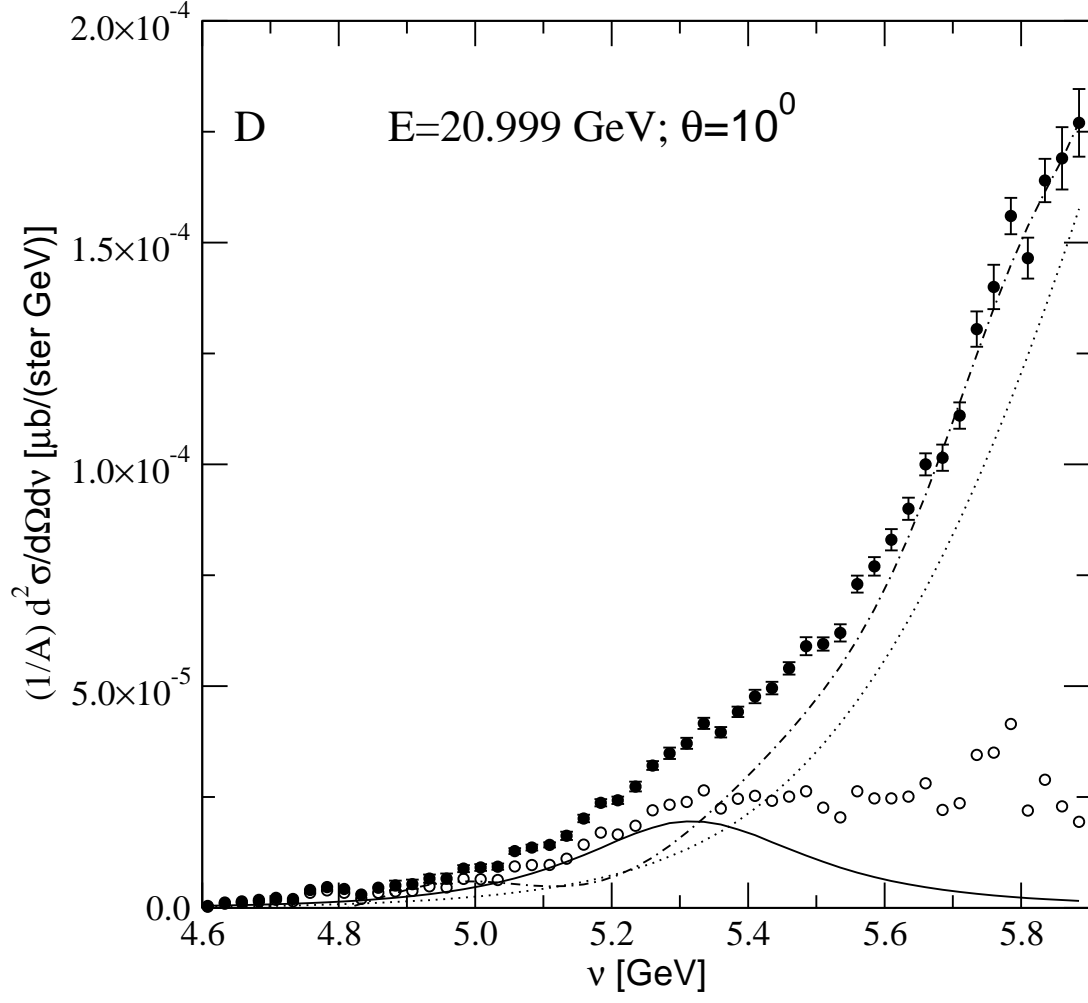


FIG. 12: As Fig. 1 for D at $E = 20.999 \text{ GeV}$, $\theta = 10^\circ$. $\bar{Q}^2 = 10.06 \text{ GeV}^2$. SLAC E133 data [50]. NE curve for $\alpha_n = 0.769$.

TABLE I: Extraction of $\alpha_n(Q^2)$ from QE inclusive scattering data on D, ^4He . Columns 1-3 give the target, beam energy E and scattering angle θ . Columns 4-6 indicate the ranges of ν, x, Q^2 , selected for the analysis of the QE and pseudo-resonance region, and \bar{Q}^2 at the QEP. The last column gives the number of points, selected for the extraction of $\langle\alpha_n(\bar{Q}^2)\rangle$, its average (with $Q^2 \rightarrow \bar{Q}^2$ for identification and error of the mean for the new, respectively the old FF parametrization).

target	E [GeV]	θ	ν [GeV]	x	Q^2 [GeV ²]; \bar{Q}^2	n [$\langle\alpha_n(\bar{Q}^2)\rangle_O$; [$\langle\alpha_n(\bar{Q}^2)\rangle_N$]]
^4He [4]	2.02	20°	0.120-0.435	2.054-0.473	0.463-0.386; 0.434	5 1.011±0.032; 1.008±0.032
	3.595	16°	0.180-0.750	2.814-0.563	0.951-0.792; 0.873	11 1.006±0.045; 0.954±0.045
	3.595	20°	0.255-0.870	3.024-0.723	1.450-1.180; 1.270	8 0.940±0.031; 0.865±0.030
^4He [2]	2.7	15°	0.139-0.784	1.806-0.239	0.471-0.352; 0.453	4 1.120±0.035; 1.114±0.036
	3.3	15°	0.099-0.858	3.872-0.341	0.720-0.549; 0.662	4 1.064±0.029; 1.031±0.029
	3.6	15°	0.100-0.793	4.573-0.462	0.859-0.689; 0.781	7 1.028±0.037; 0.982±0.038
	3.9	15°	0.104-0.698	5.167-0.649	1.009-0.851; 0.907	10 1.007±0.034; 0.950±0.034
	4.3	15°	0.191-1.000	3.357-0.515	1.204-0.967; 1.090	9 0.978±0.033; 0.912±0.033
^4He [2]	0.9	85°	0.316-0.696	1.617-0.256	0.959-0.335; 0.78	5 1.014±0.030; 1.009±0.029
	1.1	85°	0.492-0.796	1.322-0.408	1.221-0.610; 1.09	5 0.994±0.062; 0.979±0.062
R_T^{He}			0.390-0.600	1.298-0.659	0.950-0.741; 0.90	5 1.079±0.006; 1.066±0.006
D [2, 3]	4.045	15°	0.405-1.185	1.320-0.355	1.003-0.789; 0.972	10 1.004±0.023; 0.945±0.024
	4.045	23°	0.615-1.575	1.911-0.537	2.206-1.589; 1.940	9 0.994±0.019; 0.921±0.021
	4.045	30°	0.930-2.505	1.933-0.355	3.376-1.669; 2.774	9 0.991±0.017; 0.915±0.019
	4.045	37°	1.245-1.935	1.951-0.946	4.561-3.437; 3.535	9 0.959±0.019; 0.874±0.020
	4.045	45°	1.695-2.505	1.750-0.776	5.568-3.649; 4.251	12 0.936±0.030; 0.845±0.035
	4.045	55°	2.160-3.045	1.603-0.603	6.502-3.449; 4.900	7 0.879±0.018; 0.789±0.018
D [48]	5.507	15.15°	0.698-1.309	1.404-0.654	1.840-1.606; 1.750	11 1.008±0.027; 0.933±0.026
	5.507	18.98°	1.011-1.665	1.418-0.736	2.692-2.300; 2.500	17 0.998±0.039; 0.919±0.040
	5.507	22.81°	1.571-2.053	1.149-0.771	3.388-2.973; 3.250	17 0.987±0.049; 0.900±0.051
	5.507	26.82°	1.983-2.424	1.121-0.803	4.176-3.653; 4.000	6 0.951±0.058; 0.851±0.059
R_T^D			0.773-0.971	1.066-0.950	1.769-1.733; 1.750	10 0.957±0.023; 0.940±0.024
			1.281-1.394	1.051-0.940	2.529-2.461; 2.500	5 0.973±0.022; 0.957±0.022
			1.692-1.838	1.034-0.942	3.286-3.188; 3.250	7 0.978±0.018; 0.959±0.018
			2.095-2.210	1.027-0.941	4.059-3.905; 4.000	4 0.901±0.025; 0.866±0.025
D [47]	2.015	38.84°	0.582-0.722	1.168-0.850	1.277-1.152; 1.22	7 0.924±0.033; 0.868±0.036
	3.188	47.68°	1.635-1.786	1.054-0.871	3.235-2.921; 3.15	4 0.956±0.089; 0.897±0.096
	4.212	53.39°	2.659-2.810	1.058-0.904	5.280-4.767; 5.10	6 0.855±0.064; 0.774±0.070
	5.120	56.64°	3.567-3.719	1.069-0.928	7.156-6.461; 6.83	4 0.842±0.051; 0.786±0.049
D [50]	9.744	10°	1.14-1.60	1.19-0.803	2.547-2.4112; 2.50	6 0.977±0.056; 0.878±0.061
	12.565	10°	1.821-2.537	1.200-0.804	4.101-3.828; 4.00	7 0.913±0.050; 0.784±0.053
	15.730	10°	2.758-3.768	1.197-0.808	6.199-5.716; 6.00	10 0.854±0.029; 0.714±0.031
	17.301	10°	3.274-4.331	1.200-0.838	7.373-6.817; 7.12	8 0.879±0.124; 0.812±0.117
	18.476	10°	3.087-4.748	1.191-0.864	8.289-7.705; 8.03	9 0.958±0.038; 0.912±0.038
	20.999	10°	4.658-5.885	1.192-0.873	10.424-9.642; 10.06	5 0.769±0.118; 0.708±0.131

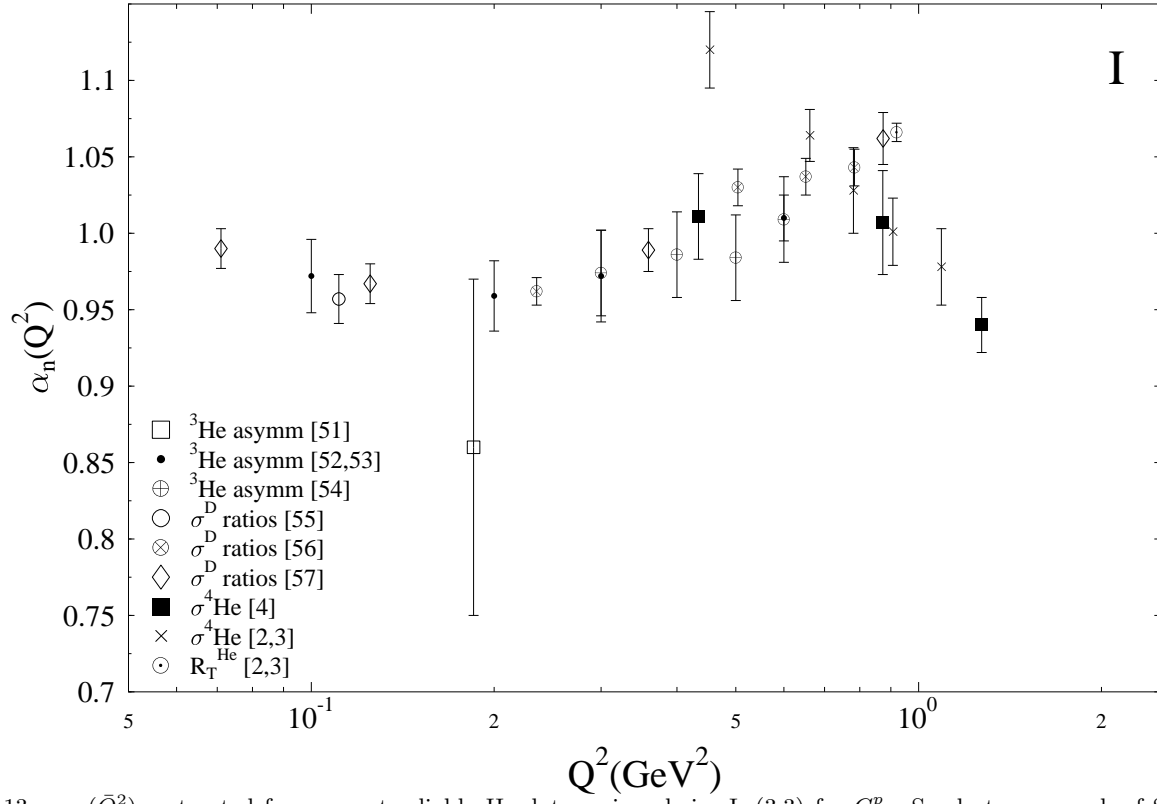


FIG. 13: $\alpha_n(\bar{Q}^2)$, extracted from recent reliable He data, using choice I, (3.3) for G_E^p . See last paragraph of Section V for description.

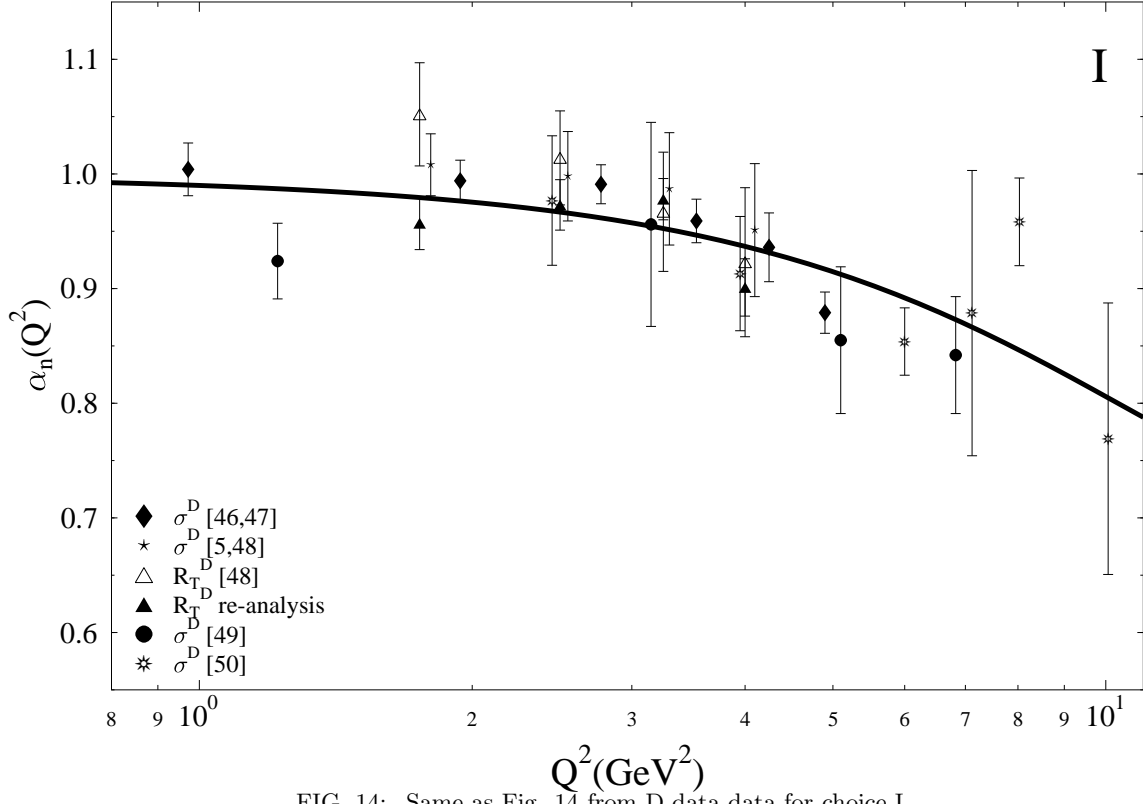


FIG. 14: Same as Fig. 14 from D data data for choice I.

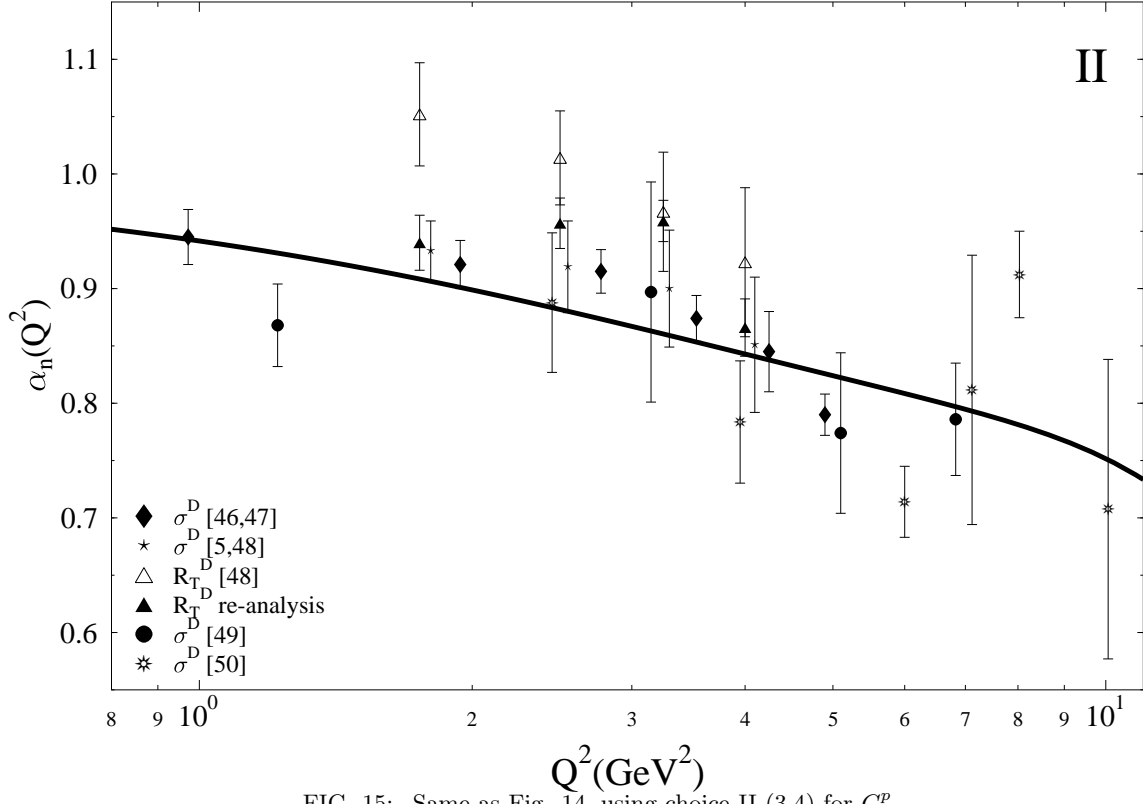


FIG. 15: Same as Fig. 14, using choice II (3.4) for G_E^p .